Advanced scalar intensity measures for collapse capacity prediction of steel moment resisting frames with fluid viscous dampers

H.R. Jamshidiha, M. Yakhchalian*, B. Mohebi

Department of Civil Engineering, Faculty of Engineering and Technology, Imam Khomeini International University, PO Box 34149-16818, Qazvin, Iran

ABSTRACT

Nowadays, passive energy dissipation systems are used in the seismic design of new structures and the retrofit of existing structures. Fluid Viscous Dampers (FVDs) are one of the important types of passive energy dissipation systems. Using FVDs can considerably decrease the seismic demands on structures. In this study, seismic collapse behavior of steel Special Moment Resisting Frames (SMRFs) equipped with FVDs is investigated using different scalar Intensity Measures (IMs). Incremental Dynamic Analysis (IDA) method is applied to determine the collapse capacity, IM_{col}, values for low- to mid-rise steel SMRFs equipped with FVDs. After determining the collapse capacity, IM_{col}, values by using each of the IMs, the efficiency and sufficiency of the IMs for predicting the seismic collapse capacity of the structures are investigated. Then, advanced scalar IMs, including the effects of spectral shape and ground motion duration, are proposed to reliably predict the collapse capacity of steel SMRFs equipped with FVDs. The results indicate that the proposed IMs possess high efficiency and sufficiency for collapse capacity prediction of steel SMRFs equipped with FVDs.

1. Introduction

Using passive energy dissipation systems, including Fluid Viscous Dampers (FVDs), hysteretic dampers, viscoelastic dampers and friction dampers, is one of the effective ways to mitigate excitations due to strong ground motions [1,2]. FVDs are a type of passive energy dissipation systems that are extensively used for the seismic design of new structures and the retrofit of existing structures [3,4]. For elastic structures, using FVDs reduces both displacements and accelerations simultaneously [5,6]. However, as pointed out by Karavasilis and Seo [7], for highly inelastic structures, FVDs may increase accelerations, as the damper forces are not out of phase with the peak drifts and internal member forces, due to the nonlinearity of the structure. FVDs provide a velocity-dependent force and can behave as linear or nonlinear elements. The force developed by a FVD is as follows:

$$F_d = C \cdot |v|^{\alpha_d} \cdot \text{sgn}(v) \qquad (1)$$

where C is the damper coefficient, v is the relative velocity between the two ends of the damper, α_d is the velocity exponent, and sgn is the signum function. In seismic applications, the exponent α_d is in the range of 0.2–1.0 [8]. When α_d is equal to one, the damper is called "linear FVD", and values of α_d lower than one represent nonlinear FVDs.

Several researchers have investigated the seismic response of structures equipped with FVDs (e.g., see [9,10]). Although a number of

procedures have been developed for the design of these structures [11–13], the seismic collapse of these structures has not been extensively investigated. The collapse of structural systems due to strong ground motions is the primary source of casualties and loss of life during earthquakes. Seismic collapse occurs when a structural system is unable to withstand gravity loads under earthquake shaking. In recent years, due to significant advancements in the computational capability of computers and the methods of nonlinear analysis, assessing the seismic collapse of structures has become an interesting field of study for researchers. Thus, several studies have been performed to assess the seismic collapse of structures [14–16], and to develop engineering approaches for seismic collapse assessment. The ATC-63 document [17] presents a new methodology for seismic collapse assessment of structures, to assess design criteria and seismic performance factors existing in seismic codes. Recently, some studies have been performed to assess the seismic collapse of structures equipped with FVDs. For instance, Hamidia et al. [18] proposed a simplified approach to assess the seismic collapse of structures equipped with FVDs. Seo et al. [19] investigated the seismic resistance of steel Moment Resisting Frames (MRFs) with supplemental FVDs against collapse. They observed that in some cases, the collapse mode consists of a combination of beam and column plastic hinges. Karavasilis [20] investigated the effects of column capacity design rules on the collapse performance of MRFs with FVDs. He showed that taller steel MRFs (i.e., 10-story and 20-story MRFs) are

---

prone to column plastic hinging.

Intensity Measure (IM) is a parameter that describes the strength of a ground motion and quantifies its effect on structures. In fact, an IM links the output of the ground motion hazard analysis to the seismic response of structure. An optimal IM should meet the requirements of efficiency and sufficiency [21]. In other words, efficiency and sufficiency are the main desirable features of an optimal IM. Efficiency is the ability of an IM to predict the response or capacity of a structure subjected to ground motion with small dispersion, whereas sufficiency is the ability of an IM to predict the response or capacity of a structure conditionally independent of other ground motion properties. In fact, using an efficient IM leads to smaller variability in the structural response or capacity prediction, which allows the use of a lower number of ground motion records in seismic analyses. Moreover, using a sufficient IM reduces the complexity of record selection procedure, because no other ground motion information (i.e., magnitude, source-to-site distance, etc.) is required to predict the structural response or capacity [22,23]. To determine the seismic response or capacity of a structure, ground motion records are scaled, and thus the results may become biased due to record scaling. Another desirable feature of an optimal IM is scaling robustness, which means that the IM is sufficient with respect to Scale Factor (SF), when predicting the response or capacity of a structure [23,24]. The last desirable feature of an optimal IM is predictability, that is, the IM should be predictable using a Ground Motion Prediction Equation (GMPE).

In general, IMs are classified into two groups of scalar and vector (e.g., see [25,26]). Common scalar IMs are spectral acceleration at the fundamental period of structure, $Sa(T_1)$, Peak Ground Acceleration (PGA), Peak Ground Velocity (PGV) and Peak Ground Displacement (PGD). Shome et al. [27] showed that $Sa(T_1)$ is more efficient and sufficient than PGA. Thus, nowadays, seismic codes throughout the world use $Sa(T_1)$ as the most common scalar IM. It should be noted that when a structure behaves nonlinearly, its fundamental period lengthens. Moreover, higher mode effects may have a significant contribution in the response of a structure. Therefore, spectral regions far away from the fundamental period of a structure, T_1, may play an important role in the response of the structure. Hence, some researchers have proposed more advanced scalar IMs, which contain information about the spectral shape of ground motion records. Cordova et al. [28] proposed a power-law form scalar IM consisting of $Sa(T_1)$ and the ratio of spectral acceleration at a period greater than T_1, $Sa(T_2)$, to $Sa(T_1)$ to account for the period lengthening of structures due to nonlinear deformations. Mehanny [29] enhanced this power-law form IM by defining the lengthened period, T_2, as the multiplication of a nonlinear demand dependent period multiplier by T_1. Baker [30] pointed out that in some cases, an IM which averages spectral acceleration values over a range of periods (i.e., the geometric mean of spectral accelerations over a range of periods) might be a better indicator of structural response. Bojorquez and Iervolino [31] proposed a scalar IM, I_{Np}, which is similar to the power-law form IM proposed by Cordova et al. [28] but uses the geometric mean of spectral accelerations over a range of periods (i.e., T_1 to a lengthened period) instead of $Sa(T_2)$. Although many of the studies in the field of ground motion IMs have focused on investigating the efficiency and sufficiency of IMs to predict the structural response (e.g., [21,32]), due to the importance of assessing the seismic collapse of structures, some studies have focused on investigating the efficiency and sufficiency of IMs for collapse capacity prediction (e.g., [24,33–35]). Eads et al. [34,35] indicated that the geometric mean of spectral accelerations over the period range of $0.2T_1$ to a lengthened period, $3T_1$, is a good scalar IM to predict the collapse capacity of structures. Some researchers (e.g., Chandramohan et al. [36]) showed that ground motion duration has a significant effect on the seismic collapse of structures. Therefore, combining the effect of ground motion duration with the other characteristics of ground motion records (e.g., spectral shape) may lead to advanced optimal IMs for collapse capacity prediction. In fact, using such an idea may progress the state-of-the-art

in terms of IMs for predicting the collapse capacity of steel and reinforced concrete Special Moment Resisting Frames (SMRFs). A review on the technical literature existing in the field of investigating the efficiency and sufficiency of IMs indicates that an assessment of the efficiency and sufficiency of IMs to predict the collapse capacity of SMRFs with FVDs has never been performed. Based on the results of the studies performed by Seo et al. [19] and Karavasilis [20], described previously, there may be differences between the collapse mechanisms of steel SMRFs with and without FVDs. Thus, the need for conducting an assessment of the efficiency and sufficiency of IMs to predict collapse capacity of SMRFs with FVDs can be justified.

The aim of this study is to investigate the efficiency and sufficiency of scalar IMs to predict the collapse capacity of steel SMRFs equipped with FVDs. For this aim, 12 low- to mid-rise steel SMRFs and 27 scalar IMs are considered. Then, different levels of supplemental viscous damping are added to each structure, and the collapse capacities of the structures with and without supplemental viscous damping are determined using the IMs. After investigating the efficiency and sufficiency of the IMs, three advanced scalar IMs, including the effects of spectral shape and ground motion duration, are proposed for collapse capacity prediction of the structures. To satisfy the predictability criterion for the proposed IMs, GMPEs are presented for these IMs.

2. Selected IMs

In this study, the considered scalar IMs were classified into two groups: (1) non-structure-specific IMs and (2) structure-specific IMs. Non-structure-specific IMs are obtained only from the time histories of a ground motion record, whereas to calculate structure-specific IMs the spectral components of a ground motion record are involved. It should be mentioned that all of these spectral components are estimated at 5% damping.

The first group includes acceleration-, velocity- and displacement-related IMs. The acceleration-related IMs are Peak Ground Acceleration (PGA), Arias Intensity (AI) [37], characteristic intensity, I_C, [38], the IM proposed by Riddell and Garcia, I_a, [39] and Cumulative Absolute Velocity (CAV) [40]. The velocity-related IMs are Peak Ground Velocity (PGV), Fajfar Intensity (FI) [41], the IM proposed by Riddell and Garcia, I_v, [39], Cumulative Absolute Displacement (CAD) [42] and Specific Energy Density (SED). The displacement-related IMs are Peak Ground Displacement (PGD), the IM proposed by Riddell and Garcia, I_d, [39] and Cumulative Absolute Impulse (CAI). Table 1 presents the non-structure-specific IMs and their definitions.

The second group includes $Sa(T_1)$ as the most common scalar IM, spectral shape based IMs, and combined spectral shape and duration based IMs. The spectral shape based IMs considered in this study are Acceleration Spectrum Intensity (ASI) [43], Spectrum Intensity (SI) [44,45], Displacement Spectrum Intensity (DSI) [46] (which are the integrals of pseudo-acceleration, pseudo-velocity and displacement response spectra, respectively), the power-law form scalar IM proposed by Cordova et al. [28] (IM_C), I_{Np} [31], the power-law form scalar IM proposed by Mehanny [29] (IM_M), and Sa_{avg} [34,35]. IM_C is defined as:

$$IM_C = Sa(T_1) \cdot \left(\frac{Sa(T_2)}{Sa(T_1)} \right)^{0.5} ; \quad T_2 = 2\,T_1 \tag{2}$$

where $T_2 = 2T_1$ is the lengthened period. The enhanced version of IM_C is IM_M that is defined, by changing the lengthened period, as:

$$IM_M = Sa(T_1) \cdot \left(\frac{Sa(T_2)}{Sa(T_1)} \right)^{0.5} ; \quad T_2 = R^\alpha T_1; \quad \alpha = 0.5 \text{ or } 0.33 \tag{3}$$

where R is the lateral strength required to maintain the system elastic relative to the lateral yielding strength of the system. In this study, the parameter R was assumed as follows:

Table 1
Non-structure-specific IMs considered in this study.

Notation	Name	Definition
Acceleration-related		
PGA	Peak Ground Acceleration	$PGA = \max |a(t)|$ $a(t)$ = acceleration time history
AI	Arias Intensity [37]	$AI = \frac{\pi}{2g} \int_0^{t_f} a(t)^2 dt$ t_f = total duration
I_C	Characteristic intensity [38]	$I_C = (a_{rms})^{1.5} \cdot t_d^{0.5}$ $a_{rms} = \sqrt{\frac{1}{t_d} \int_{t_1}^{t_2} a(t)^2 dt}$; $\quad t_d = t_2 - t_1$ $t_1 = t(5\% AI); \quad t_2 = t(95\% AI)$
I_a	Compound acceleration-related IM [39]	$I_a = PGA \cdot t_d^{1/3}$
CAV	Cumulative Absolute Velocity [40]	$CAV = \int_0^{t_f} |a(t)| dt$
Velocity-related		
PGV	Peak Ground Velocity	$PGV = \max |v(t)|$ $v(t)$ = velocity time history
FI	Fajfar Intensity [41]	$FI = PGV \cdot t_d^{0.25}$
I_v	Compound velocity-related IM [39]	$I_v = PGV^{2/3} \cdot t_d^{1/3}$
CAD	Cumulative Absolute Displacement [42]	$CAD = \int_0^{t_f} |v(t)| dt$
SED	Specific Energy Density	$SED = \int_0^{t_f} v(t)^2 dt$
Displacement-related		
PGD	Peak Ground Displacement	$PGD = \max |d(t)|$ $d(t)$ = displacement time history
I_d	Compound displacement-related IM [39]	$I_d = PGD \cdot t_d^{1/3}$
CAI	Cumulative Absolute Impulse	$CAI = \int_0^{t_f} |d(t)| dt$

Table 2
Structure-specific IMs considered in this study.

Notation	Name	Definition
Spectral		
$Sa(T_1)$	Spectral acceleration at T_1	
Spectral shape based		
ASI	Acceleration Spectrum Intensity [43]	$ASI = \int_{0.1}^{0.5} Sa(T, 5\%) dT$
SI	Spectrum Intensity [44,45]	$SI = \int_{0.1}^{2.5} Sv(T, 5\%) dT$
DSI	Displacement Spectrum Intensity [46]	$DSI = \int_2^5 Sd(T, 5\%) dT$
IM_C		Eq. (2)
IM_M		Eq. (3)
I_{Np}		Eq. (5)
Sa_{avg}		Eq. (6)
Combined Spectral shape and duration based		
IM_{C-D}		$IM_{C-D} = Sa(T_1) \cdot \left(\frac{Sa(2T_1)}{Sa(T_1)} \right)^{0.5} \cdot t_d^{\beta}$
IM_{M-D}		$IM_{M-D} = Sa(T_1) \cdot \left(\frac{Sa(R^{\alpha}T_1)}{Sa(T_1)} \right)^{m} \cdot t_d^{\beta}$
I_{Np-D}		$I_{Np-D} = Sa(T_1) \cdot Np^{0.4} \cdot t_d^{\beta}$
$I_{Np\ M-D}$		$I_{Np\ M-D} = Sa(T_1) \cdot \left(\frac{Sa_{avg}(T_1...T_N)}{Sa(T_1)} \right)^{n} \cdot t_d^{\beta}$ $T_N = R^{\alpha} T_1$
Sa_{avg-D}		$Sa_{avg-D} = Sa_{avg}(c_1 T_1 ... c_N T_1) \cdot t_d^{\beta}$ $c_1 = 0.2; \quad c_N = 3$
$Sa_{avg\ M-D}$		$Sa_{avg\ M-D} = Sa_{avg}(c_1 T_1 ... c_N T_1) \cdot t_d^{\beta}$ $c_N = R^{\alpha}$

$$R = \frac{Sa(T_1)/g}{B \cdot \gamma} \tag{4}$$

where g is the acceleration of gravity, γ is the ratio of fully yielded strength, V_y, [47] to weight, $\gamma = V_y/W$, and B is the damping coefficient, which can be determined based on the values proposed by Ramirez et al. [11]. The scalar IM I_{Np}, proposed by Bojorquez and Iervolino [31], is defined as:

$$I_{Np} = Sa(T_1) \cdot Np^{0.4}; \quad Np = \frac{Sa_{avg}(T_1 ... T_N)}{Sa(T_1)} \tag{5}$$

where Np is a spectral shape proxy, $Sa_{avg}(T_1...T_N)$ is the geometric mean of spectral accelerations over the period range of T_1–T_N, and T_N is a lengthened period equal to $2T_1$. It should be noted that Np and $Sa(T_2)/Sa(T_1)$ indicate the shape of pseudo-acceleration response spectrum in periods greater than the fundamental period of structure. Thus, when the fundamental period of a structure lengthens due to nonlinear deformations, IM_C, IM_M and I_{Np} can imply the severity of ground motion more realistically, compared with $Sa(T_1)$. The IM Sa_{avg}, proposed by Eads et al. [34,35], which includes both the effects of higher modes and period lengthening due to nonlinear deformations, is defined as:

$$Sa_{avg} = Sa_{avg}(c_1 T_1 ... c_N T_1) = \left(\prod_{i=1}^{N} Sa(c_i T_1) \right)^{1/N}; \quad c_1 = 0.2; c_N = 3. \tag{6}$$

In this IM, the lengthened period is equal to $3T_1$. The combined spectral shape and duration based IMs considered in this study are IM_{C-D}, IM_{M-D}, I_{Np-D}, $I_{Np\ M-D}$, Sa_{avg-D} and $Sa_{avg\ M-D}$, which are based on the idea of adding the effect of ground motion duration to the spectral shape based IMs, and are defined by multiplying these IMs, except the integral based

IMs, by a power function of significant duration, t_d^{β}. The significant duration, t_d, is the time interval between 5% and 95% contributions to the integral of square acceleration [48]. Table 2 presents the structure-specific IMs and their definitions. For the IMs IM_{M-D}, $I_{Np\ M-D}$ and $Sa_{avg\ M-D}$, the lengthened period was considered as $R^{\alpha}T_1$.

In this study, sensitivity analyses were performed to obtain the optimal values of β for the IMs IM_{C-D}, I_{Np-D} and Sa_{avg-D} by simultaneously accounting for the efficiency and sufficiency criteria. For this purpose, the value of β was varied in the range of -0.5 to 0.5 in increments of 0.01. Furthermore, sensitivity analyses were performed to obtain the optimal values of the parameters for the IMs IM_{M-D}, $I_{Np\ M-D}$ and $Sa_{avg\ M-D}$ (i.e., the parameters α, β and m for IM_{M-D}, α, β and n for $I_{Np\ M-D}$, and α, β and c_1 for $Sa_{avg\ M-D}$). For this aim, the values of m, n and c_1 were varied from 0 to 1.0 in increments of 0.1. Given a value of m, n or c_1, the values of α and β were respectively varied from 0 to 0.5 and -0.5 to 0.5 in increments of 0.01, and the optimal values of α, β were determined by simultaneously accounting for the efficiency and sufficiency criteria for the IM considered (i.e., IM_{M-D}, $I_{Np\ M-D}$ or $Sa_{avg\ M-D}$). Then, comparing the results from optimal values of α and β given different values of m, n or c_1, the optimal values of the parameters for each of the IMs were selected. The results of the sensitivity analyses are briefly presented in Sections 4 and 5. To summarize the results, given the final selected optimal values of m, n and c_1 for the IMs IM_{M-D}, $I_{Np\ M-D}$ and $Sa_{avg\ M-D}$, respectively, only the results from varying the values of α and β on the efficiency and sufficiency of these IMs are presented. It should be noted that when the value of α is zero, the IMs IM_{M-D}, $I_{Np\ M-D}$ are simplified to $Sa(T_1) \cdot t_d^{\beta}$, and when the values of α and β are zero, these IMs are simplified to $Sa(T_1)$.

3. Structural modeling and analysis

In this study, 3- 6- and 9-story code-designed steel SMRFs, used by Hamidia et al. [18], were selected. These benchmark structures were designed for the SAC steel project [49], and their detailed information can be found in FEMA 355C [50] and the study by Hall [51]. In order to derive more structures form the benchmark structures, some changes,

including changes in structural height or seismic mass, were performed on these structures. The story heights of the 3-story structure were increased uniformly by factors of 1.2 and 1.4, and 3-story-h1.2 and 3-story-h1.4 structures were generated, respectively. Furthermore, because the story heights in the 3-story structure are identical, the first story height of this structure was increased by factors of 1.2 and 1.4, and 3-story-$h_1$1.2 and 3-story-$h_1$1.4 structures were generated, respectively. In the case of the 6- and 9-story structures, the first story height is greater than the typical story height (h_{typ}). Thus, h_{typ} in the 6-story structure was increased by factors of 1.2 and 1.4 and 6-story-h_{typ}1.2 and 6-story-h_{typ}1.4 structures were generated, respectively. Moreover, h_{typ} in the 9-story structure was increased by a factor of 1.2 and 9-story-h_{typ}1.2 structure was generated. The seismic mass of the 3-story structure was also uniformly increased by factors of 1.2 and 1.4, and 3-story-m1.2 and 3-story-m1.4 structures were generated, respectively. Thus, 12 structures were considered.

OpenSees software [52] was used to create the 2D numerical models of the structures. Distributed plasticity force-based beam-column elements consisting of five integration points, each using a fiber section, along the element length were used to model the columns. "Steel02" material in OpenSees, assuming E = 200 GPa and a strain hardening ratio of 0.002, was applied to model the uniaxial behavior of each fiber. Thus, cyclic deterioration in the column elements was neglected. The same ratio of low strain hardening was also used by other researchers [19,53]. The reason for using the distributed plasticity approach to model the columns, which were selected from W14 sections, is that according to the tests performed by Newell and Uang [54], W14 columns do not encounter deterioration in strength by more than 10% for axial loads less than 75% of the nominal yield strength of column, even at large interstory drift ratios. Thus, the main phenomenon that should be considered in the modeling of such columns is the interaction between moment and axial load. The behavior of the beams was modeled using a concentrated plasticity approach (e.g., see Ibarra and Krawinkler [15], and Haselton [16]). Therefore, each beam was modeled using two zero-length rotational springs at its both ends, representing plastic hinges, and an elastic beam-column element. The modified Ibarra-Krawinkler model (Bilin) [55] was used to model the moment-rotation relationship of the rotational springs. This model takes into account the effects of strength and stiffness deterioration in beams, which are necessary to be considered for reliable seismic collapse assessment of steel SMRFs. The parameters of this model were determined based on the relationships proposed by Lignos and Krawinkler [55]. It is worth mentioning that other researchers (e.g., [19,20]) have also applied the distributed and concentrated plasticity approaches to model the columns and beams in steel SMRFs, respectively. In order to consider the rigid end offsets of the beams and columns, rigid elements were used at the ends of the beams and columns. The joint offsets for the beams and columns were assumed equal to the half of the column section depth and beam section depth, respectively. A leaning column was used to model the P-Δ effects of gravity columns. This leaning column was modeled by using elastic beam-column elements, which have moments of inertia and areas about two orders of magnitude larger than the frame columns. These beam-column elements were connected to the nodes in the floor levels by zero-length rotational spring elements with very small stiffness values. Then, these nodes were connected to the SMRF by axially rigid truss elements. In fact, due to using rotational springs with negligible stiffness between the ends of the beam-column elements making the leaning column and the nodes in the floor levels, the lateral stiffness of the leaning column is negligible.

Table 3 presents the first mode periods of the structures considered in this study. To compute the value of γ for a structure, the capacity curve of the structure was obtained using static pushover analysis, assuming a lateral load pattern proportional to the first mode shape of the structure. Then, the value of fully yielded strength, V_y, which is the maximum base shear in the capacity curve, was determined. Fig. 1 illustrates the capacity curves for the 12 steel SMRFs, in the form of base

Table 3
First mode periods of the structures.

Structure	First mode period (s)
3-story	0.95
6-story	1.32
9-story	2.08
3-story-h1.2	1.2
6-story-h_{typ}1.2	1.54
9-story-h_{typ}1.2	2.51
3-story-h1.4	1.47
6-story-h_{typ}1.4	1.78
3-story-$h_1$1.2	1.06
3-story-$h_1$1.4	1.2
3-story-m1.2	1.05
3-story-m1.4	1.13

shear coefficient (V_b/W)–roof drift ratio. Each graph in this figure consists of normalized pushover curves for the structures with the same number of stories. It can be seen that each of the three benchmark SMRFs has a higher normalized base shear capacity compared with the SMRFs derived from it. It should be mentioned that adding supplemental viscous damping to each of the three benchmark SMRFs leads to a higher performance than that of the corresponding benchmark code-designed SMRF. Among the other nine structures considered, those generated by increasing story height are representatives of more flexible structures, which have slightly higher ratios of code-based elastic spectral demand to γ compared with that of the corresponding benchmark structure. However, the main problem of these structures is that they do not satisfy code-based drift limit and are more vulnerable to the P-Δ effects. It is noteworthy that in the case of the 3-story-$h_1$1.2 and 3-story-$h_1$1.4 structures, the increased height of the first story drastically increases the ductility demand at this soft story. Moreover, the 3-story-m1.2 and 3-story-m1.4 structures, generated by increasing story mass, are weaker than the corresponding benchmark structure so that they are more vulnerable to the P-Δ effects. Therefore, adding supplemental viscous damping to these nine structures can be used as a way to mitigate the aforementioned problems and improve their seismic performance.

Rayleigh viscous damping was used to model the inherent viscous damping of the structures. Thus, a five percent damping ratio was assigned to the first and third mode (i.e., the mode at which the cumulative mass participation ratio exceeds 0.95) periods of the structures. In addition to the 12 SMRFs considered, assuming three levels of supplemental viscous damping ratio (i.e., $\xi_v = 0.05$, 0.1 and 0.15), linear and nonlinear FVDs were added to the SMRFs to improve their performance under seismic excitations. For each level of supplemental viscous damping ratio, four values of velocity exponent (i.e., $\alpha_d = 0.25$, 0.5, 0.75 and 1.0) were assumed. In other words, 12 structures without supplemental viscous damping and 144 (12 × 3 × 4) structures with supplemental viscous damping were considered. Fig. 2 indicates the dimensions of the three benchmark structures, and the configuration of FVDs in these structures.

The supplemental viscous damping ratio for the first mode of a structure with FVDs can be calculated as [11]:

$$\xi_v = \frac{\sum_{j=1}^{N_d} (2\pi)^{\alpha_d} T_1^{2-\alpha_d} \lambda_j C_j f_j^{1+\alpha_d} D_{roof}^{\alpha_d-1} \varphi_{rj1}^{1+\alpha_d}}{8\pi^3 \sum_{i=1}^{N_s} m_i \varphi_{i1}^2} \quad (7)$$

where T_1 is the first mode period of the structure, C_j is the damper coefficient of the jth damper, f_j is a displacement magnification factor that depends on the geometrical configuration of the jth damper (for a diagonal damper with an angle of inclination θ_j, $f_j = \cos \theta_j$), D_{roof} is the roof displacement, which was assumed equal to the roof yield displacement (δ_y) [17,18], λ_j is a constant that is a function of the velocity exponent α_d [11,18], φ_{rj1} is the first mode relative displacement (interstory drift) between the two ends of the jth damper in the horizontal
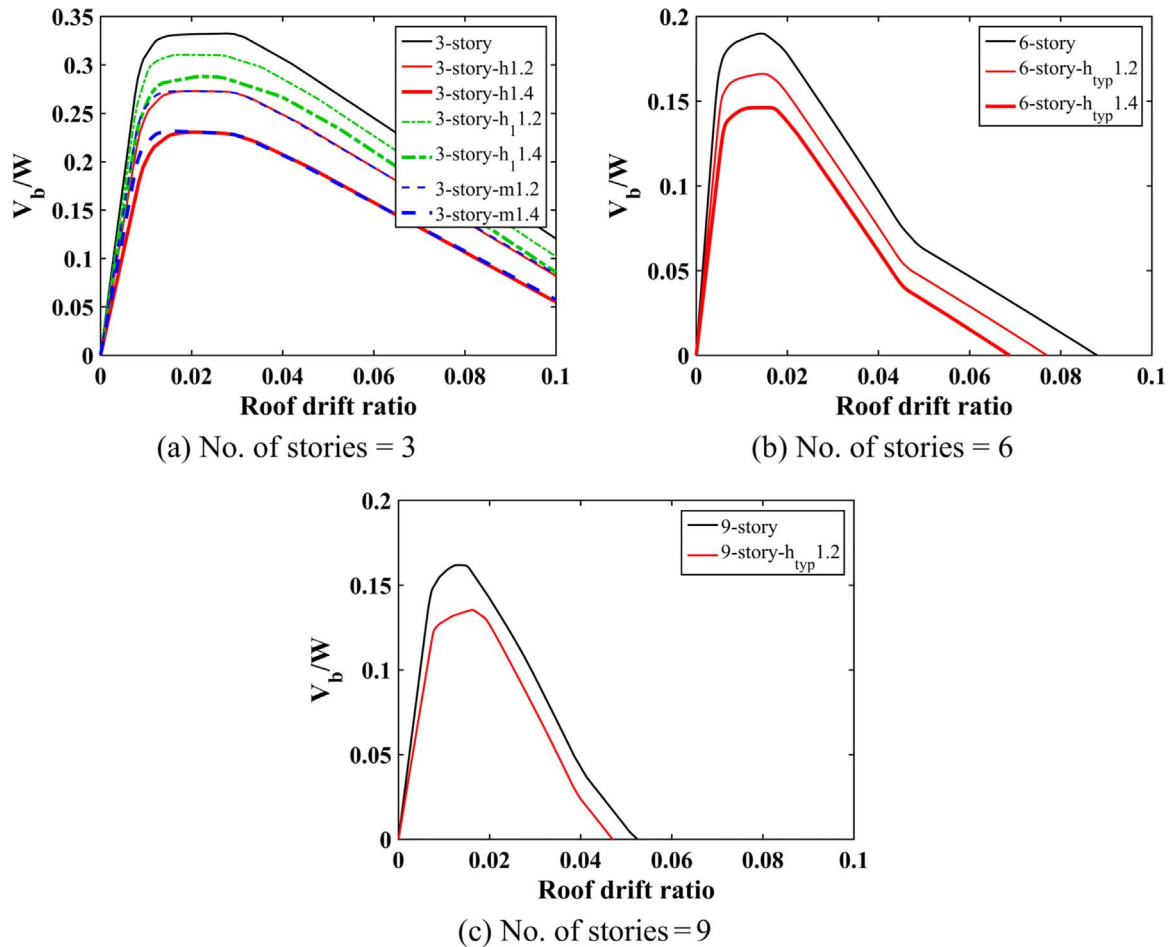
Fig. 1. Base shear coefficient (V_b/W)–roof drift ratio curves for the 12 steel SMRFs considered: (a) No. of stories = 3, (b) No. of stories = 6 and (c) No. of stories = 9.

direction, φ_{i1} is the first mode shape value at the top of story i, normalized to have a unit component at the roof, m_i is the mass of story i, and N_d and N_s are the number of dampers and stories, respectively. Given a supplemental viscous damping ratio for the first mode of a structure, ξ_v, by assuming $C_j f_j^{1+\alpha_d}$ to be proportional to the corresponding first mode interstory drift, φ_{rj1}, and rearranging Eq. (7) the following equation can be obtained to determine the damper coefficient of the kth damper:

$$C_k = \frac{8\pi^3 \, \xi_v \, \varphi_{rk1} \, \sum_{i=1}^{N_s} m_i \, \varphi_{i1}^2}{(2\pi)^{\alpha_d} \, T_1^{2-\alpha_d} \, \lambda \, f_k^{1+\alpha_d} \, D_{roof}^{\alpha_d-1} \sum_{j=1}^{N_d} \, \varphi_{rj1}^{2+\alpha_d}}. \tag{8}$$

Thus, having the assumed values of ξ_v and α_d, the values of C_k for the dampers in each of the 144 structures with supplemental viscous damping were determined using Eq. (8). To model the FVDs, it was assumed that the supporting brace member is rigid, and the dampers do not reach their stroke limits during seismic loading.
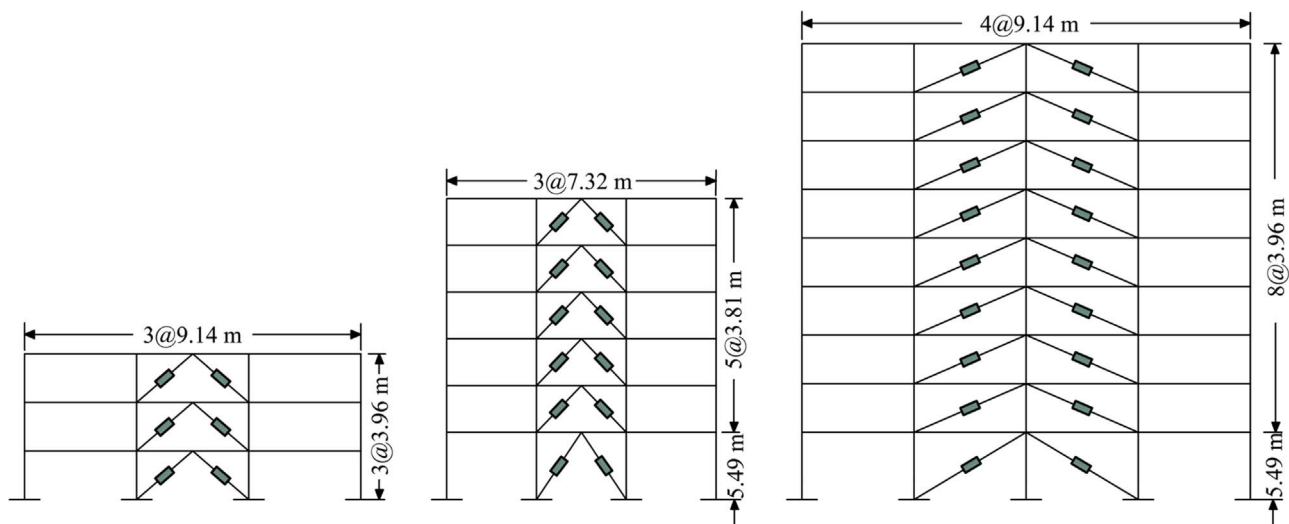

Fig. 2. Dimensions of the benchmark structures and the configuration of FVDs in these structures.
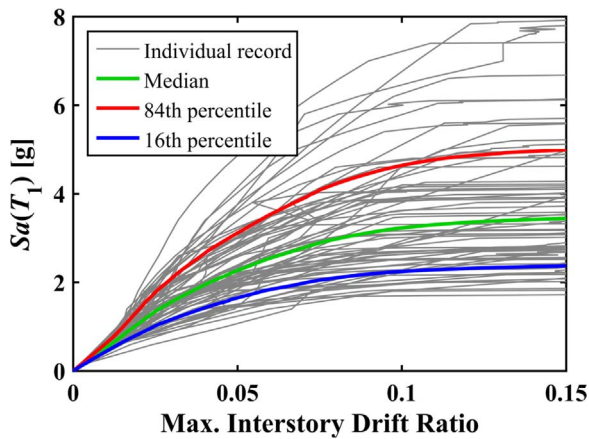
Fig. 3. IDA curves of the 3-story structure with linear FVDs and a supplemental viscous damping ratio of 0.1.

To determine the collapse capacities of the structures using Incremental Dynamic Analysis (IDA) method [14], 67 high-amplitude ground motion records used by Yakhchalian et al. [24,56], which may cause the structural collapse of code-compliant structures, were considered. These high-amplitude ground motion records are related to shallow crustal earthquakes throughout the world, and have maximum usable periods greater or equal to 5.0 s. The collapse was assumed to occur when the maximum interstory drift ratio of the structure reaches 0.15. This assumption has also been used by other researchers (e.g., [22,57]). Considering $Sa(T_1)$ as the IM for performing IDAs, the intensity of each ground motion record, $Sa(T_1)$, was incrementally scaled until the collapse occurs. Thus, the value of $Sa(T_1)$ corresponding to the collapse, Sa_{col}, was computed for each of the ground motion records. Fig. 3 illustrates the IDA curves of the 3-story structure with linear FVDs and a supplemental viscous damping ratio of 0.1. When the values of Sa_{col} for a structure were computed by using the selected ground motion records, the IM_{col} values corresponding to the other IMs were also calculated. Thus, the IM_{col} values were obtained for all of the structures. It should be mentioned that to obtain the values of IM_{col} using the IMs including the lengthened period of $R^\alpha T_1$, the value of R corresponding to each record was calculated as the ratio of Sa_{col}/g for that record to

$B \cdot \gamma$. The values of B for $\xi_v = 0.05, 0.1$ and 0.15 were determined equal to 1.2, 1.35 and 1.5, respectively, based on the values proposed by Ramirez et al. [11]. For the structures without supplemental viscous damping, the value of B is equal to 1.0.

4. Investigating the efficiency of the IMs for collapse capacity prediction

Efficiency of an IM for collapse capacity prediction is the ability of the IM to predict the collapse capacity of a structure subjected to ground motion records with small dispersion [22]. Thus, an efficient IM can predict the collapse capacity of structures with a lower record-to-record variability, which causes more accuracy in seismic collapse assessment. The logarithmic standard deviation of IM_{col} values, $\sigma_{\ln IMcol}$, which is called dispersion, is an index for the efficiency of scalar IMs for collapse capacity prediction. In other words, a lower value for $\sigma_{\ln IMcol}$ represents a more efficient IM for collapse capacity prediction. In this section, the values of dispersion, calculated using the considered IMs, are compared. It should be mentioned that to calculate the values of dispersion using the spectral shape based IMs and the combined spectral shape and duration based IMs including the lengthened period of $R^\alpha T_1$, the results of the records in which their maximum usable periods were lower than the lengthened periods of the IMs were omitted. Moreover, if the lengthened period of an IM_{col} value corresponding to a record was greater than 10.0 s, then the IM_{col} value was omitted. The reason for the omission of these results is that at the periods greater than the maximum usable period of the record, the spectral shape of the record has been suppressed such that it is not representative of the real ground motion. In addition, GMPEs for spectral accelerations are often valid up to a period of 10.0 s. It is worth mentioning that another strategy could be using the minimum of $R^\alpha T_1$, 10.0 s and the maximum usable period of the record as the lengthened period of the IM. In this study, these two strategies were investigated and nearly identical results were obtained. Thus, the results obtained using the first strategy are presented. Table 4 presents the mean values of dispersion, $(\sigma_{\ln IMcol})_{avg}$, calculated considering all of the structures, using the non-structure-specific IMs, and also the structure-specific IMs except the combined spectral shape and duration based IMs. The results indicate that I_v, IM_M ($\alpha = 0.5$), IM_M ($\alpha = 0.33$) and Sa_{avg} are the most efficient IMs, respectively.

Table 4

Results from investigating the efficiency and sufficiency of the IMs to predict the collapse capacity of the structures.

| IM	Mean value of dispersion, $(\sigma_{\ln IMcol})_{avg}$	Coefficient of variation for $\sigma_{\ln IMcol}$ values	% of structures with p-values ≥ 0.05			
			M	R	Vs30	SF
PGA	0.61	0.0752	45.51	100	0	0
AI	0.91	0.0991	21.15	100	0	0
CAV	0.42	0.0519	92.95	100	5.13	0
I_C	0.74	0.1069	3.21	100	5.13	0
I_a	0.52	0.0613	86.54	100	0	0
PGV	0.35	0.0994	100	100	95.51	0
FI	0.31	0.0679	76.92	100	87.18	0
I_v	0.21	0.0985	30.13	100	90.38	0
CAD	0.41	0.1333	7.69	100	100	98.08
SED	0.60	0.0938	48.08	100	96.15	0
PGD	0.53	0.0777	0	100	97.44	60.90
I_d	0.59	0.0959	0	100	100	100
CAI	0.80	0.0808	0	100	100	100
$Sa(T_1)$	0.39	0.1283	42.95	100	100	13.46
ASI	0.66	0.0682	6.41	100	3.85	0
SI	0.32	0.2316	10.90	100	100	0
DSI	0.39	0.1536	18.59	100	100	99.36
IM_C	0.29	0.1131	84.62	100	97.44	37.18
IM_M ($\alpha = 0.33$)	0.22	0.0776	84.62	100	99.36	53.85
IM_M ($\alpha = 0.5$)	0.21	0.1172	73.72	99.36	91.67	64.74
I_{Np}	0.31	0.1416	41.67	100	100	11.54
Sa_{avg}	0.25	0.1213	81.41	99.36	98.08	5.77
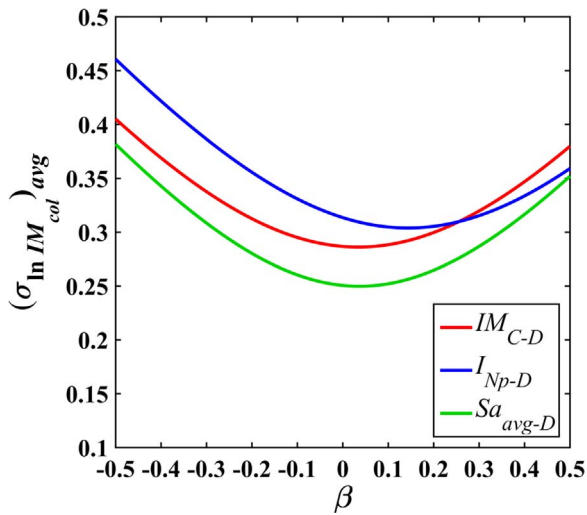
Fig. 4. Variations of $(\sigma_{\ln IMcol})_{avg}$ values for the IMs IM_{C-D}, I_{Np-D} and Sa_{avg-D} as functions of β.

Fig. 4 shows the variations of $(\sigma_{\ln IMcol})_{avg}$ values for the IMs IM_{C-D}, I_{Np-D} and Sa_{avg-D} as functions of β. It can be seen that multiplying IM_C and Sa_{avg} by t_d^{β} does not result in more efficient IMs, when compared with the initial IMs. However, multiplying I_{Np} by t_d^{β} for values of $0 < \beta < 0.3$, results in a slightly more efficient IM than I_{Np}.

To summarize the results of sensitivity analyses, given the final selected optimal values of $m = 0.5$, $n = 0.6$ and $c_1 = 0.6$ for the IMs IM_{M-D}, $I_{Np\ M-D}$ and $Sa_{avg\ M-D}$, respectively, only the results from varying the values of α and β on the efficiency and sufficiency of these IMs are presented. Fig. 5(a)–(c) illustrate the mean values of dispersion, $(\sigma_{\ln IMcol})_{avg}$, calculated using IM_{M-D}, $I_{Np\ M-D}$ and $Sa_{avg\ M-D}$, respectively, assuming different values of α and β. According to these figures, using the points (α, β) corresponding to the dark blue regions leads to more efficient IMs, when compared with the points (α, β) corresponding to the other regions. Fig. 5(a) indicates that given the point ($\alpha = 0.46$, $\beta = -0.06$), IM_{M-D} has the highest efficiency, with a $(\sigma_{\ln IMcol})_{avg}$ value of 0.21, and assuming $\beta = 0$ does not decrease the efficiency of this IM considerably. Fig. 5(b) indicates that given $\alpha = 0.5$ and $\beta = 0$, $I_{Np\ M-D}$ has the highest efficiency, which corresponds to a $(\sigma_{\ln IMcol})_{avg}$ value of 0.19. Fig. 5(c) indicates that the point ($\alpha = 0.39$, $\beta = 0.01$) corresponds to the highest efficiency for $Sa_{avg\ M-D}$ with a $(\sigma_{\ln IMcol})_{avg}$ value of 0.18, and when the value of β is zero, the value of $(\sigma_{\ln IMcol})_{avg}$ increases slightly.

(a) IM_{M-D}
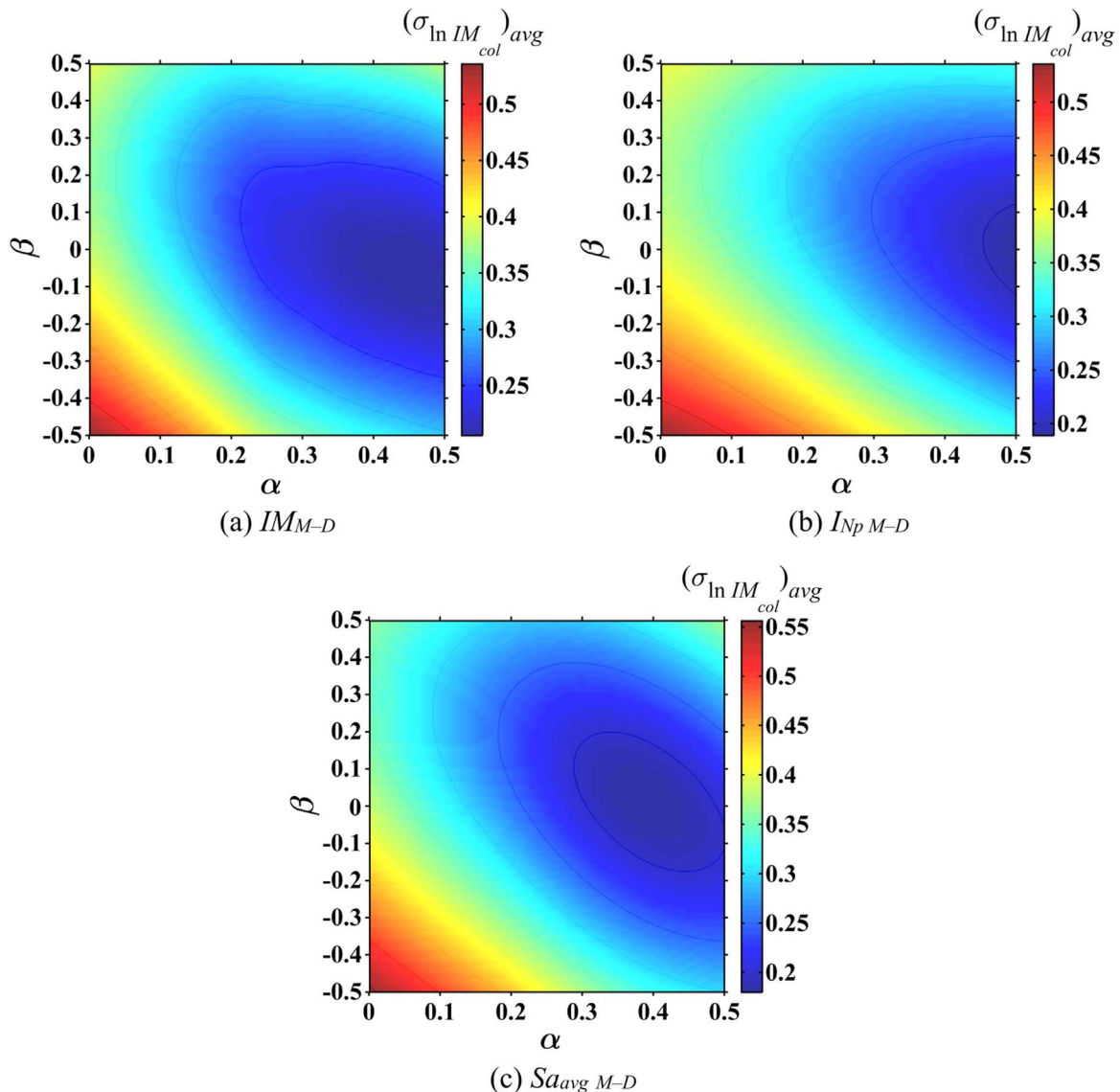

(b) $I_{Np\ M-D}$

(c) $Sa_{avg\ M-D}$

Fig. 5. Mean values of dispersion calculated using (a) IM_{M-D} given $m = 0.5$, (b) $I_{Np\ M-D}$ given $n = 0.6$, and (c) $Sa_{avg\ M-D}$ given $c_1 = 0.6$, assuming different values of α and β.
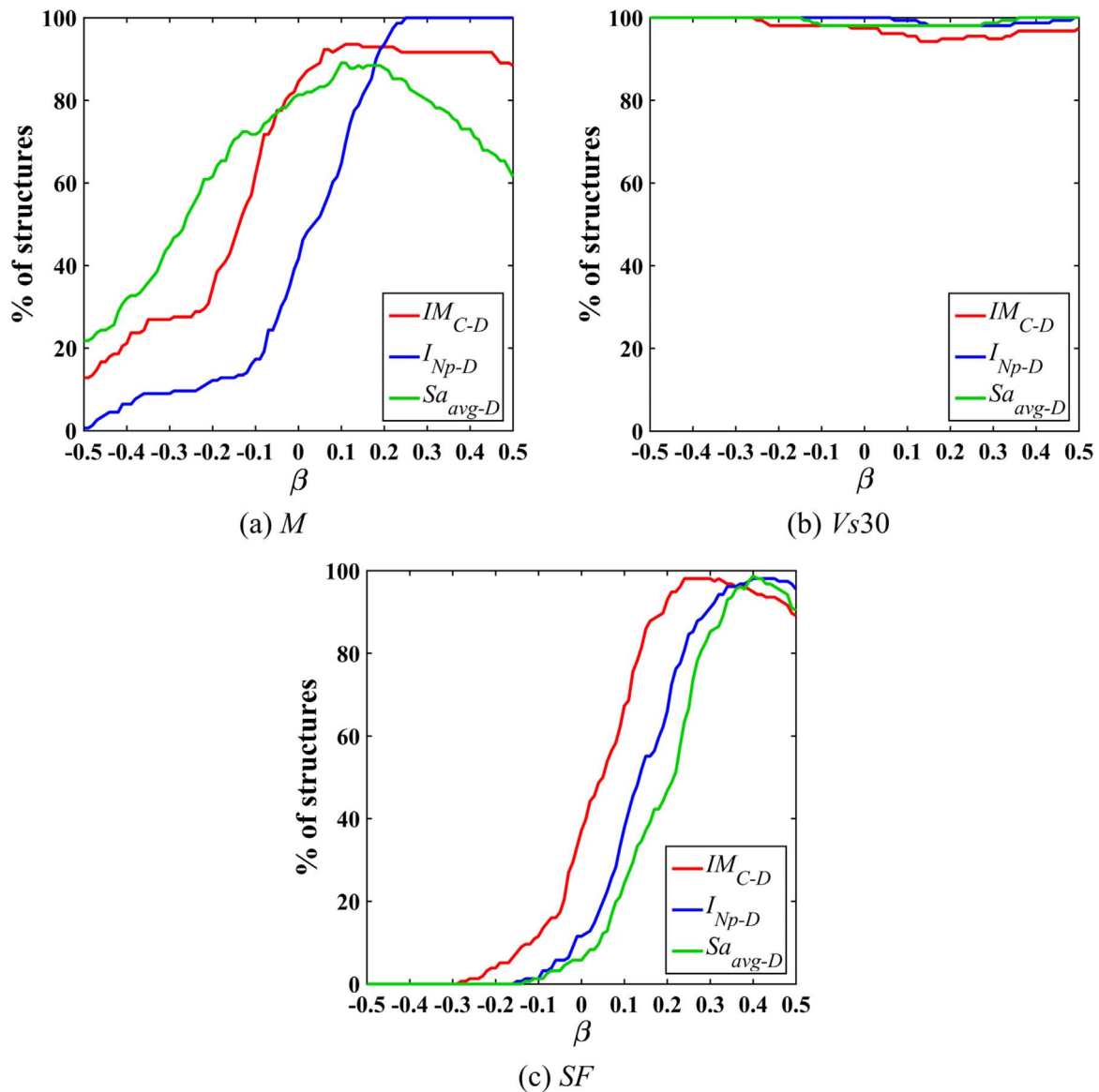
(a) M

(b) $Vs30$

(c) SF

Fig. 6. Percent of structures with p-values ≥ 0.05 obtained from investigating the sufficiency of $IM_{C–D}$, $I_{Np–D}$ and Sa_{avg_D} with respect to (a) M, (b) $Vs30$ and (c) SF as functions of β.

Based on the results, accounting for the effect of ground motion duration in the combined spectral shape and duration based IMs does not play a significant role in improving the efficiency of these IMs, when predicting the collapse capacity of the structures. It should be noted that to find the optimal values of β for use in the IMs $IM_{C–D}$, $I_{Np–D}$ and $Sa_{avg–D}$, and the optimal points (α, β) for use in the IMs $IM_{M–D}$, I_{Np} $_{M–D}$ and $Sa_{avg M–D}$, the sufficiency of the IMs should also be considered.

5. Investigating the sufficiency of the IMs for collapse capacity prediction

Sufficiency of an IM for collapse capacity prediction is the ability of the IM to predict the collapse capacity of a structure conditionally independent of other ground motion properties such as earthquake magnitude (M), source-to-site distance (R), average shear-wave velocity at the upper 30 m ($Vs30$), etc. [22]. In fact, when using a sufficient IM to predict the collapse capacity of structures, there is no need to use complex ground motion record selection procedures, because the IM represents the other ground motion properties. In order to test the sufficiency of a scalar IM with respect to a ground motion parameter (i.e., M, R, $Vs30$, etc.) for predicting the collapse capacity of structures,

a linear regression can be applied as follows:

$$E[\ln IM_{col}] = a_0 + a_1 \cdot X \tag{9}$$

where $E[\ln IM_{col}]$ is the expected value of $\ln IM_{col}$; a_0 and a_1 are the regression coefficients; and X is the earthquake magnitude, M, the natural logarithm of the source-to-site distance, $\ln R$, or the natural logarithm of the average shear-wave velocity at the upper 30 m, $\ln Vs30$, etc. The coefficient a_1 in Eq. (9) is estimated using a finite number of observations; thus, statistical tests such as F-test [58] can be used to examine the statistical significance of this coefficient. The result of the F-test is a p-value, which indicates the sufficiency or insufficiency of the IM with respect to the ground motion parameter of interest. A p-value of less than 0.05, which implies the statistical significance of the coefficient a_1, indicates the insufficiency of the considered IM, whereas a p-value of greater than 0.05 indicates the sufficiency of the considered IM. In order to test the scaling robustness of an IM, the natural logarithm of scale factor, $\ln SF$, can be substituted in Eq. (9) instead of X [24].

The results from investigating the sufficiency of the non-structure-specific IMs and also the structure-specific IMs, except the combined spectral shape and duration based IMs, for collapse capacity prediction of the structures are summarized in Table 4. To enable the reader to compare the sufficiency of the IMs with respect to M, R, $Vs30$ and SF,
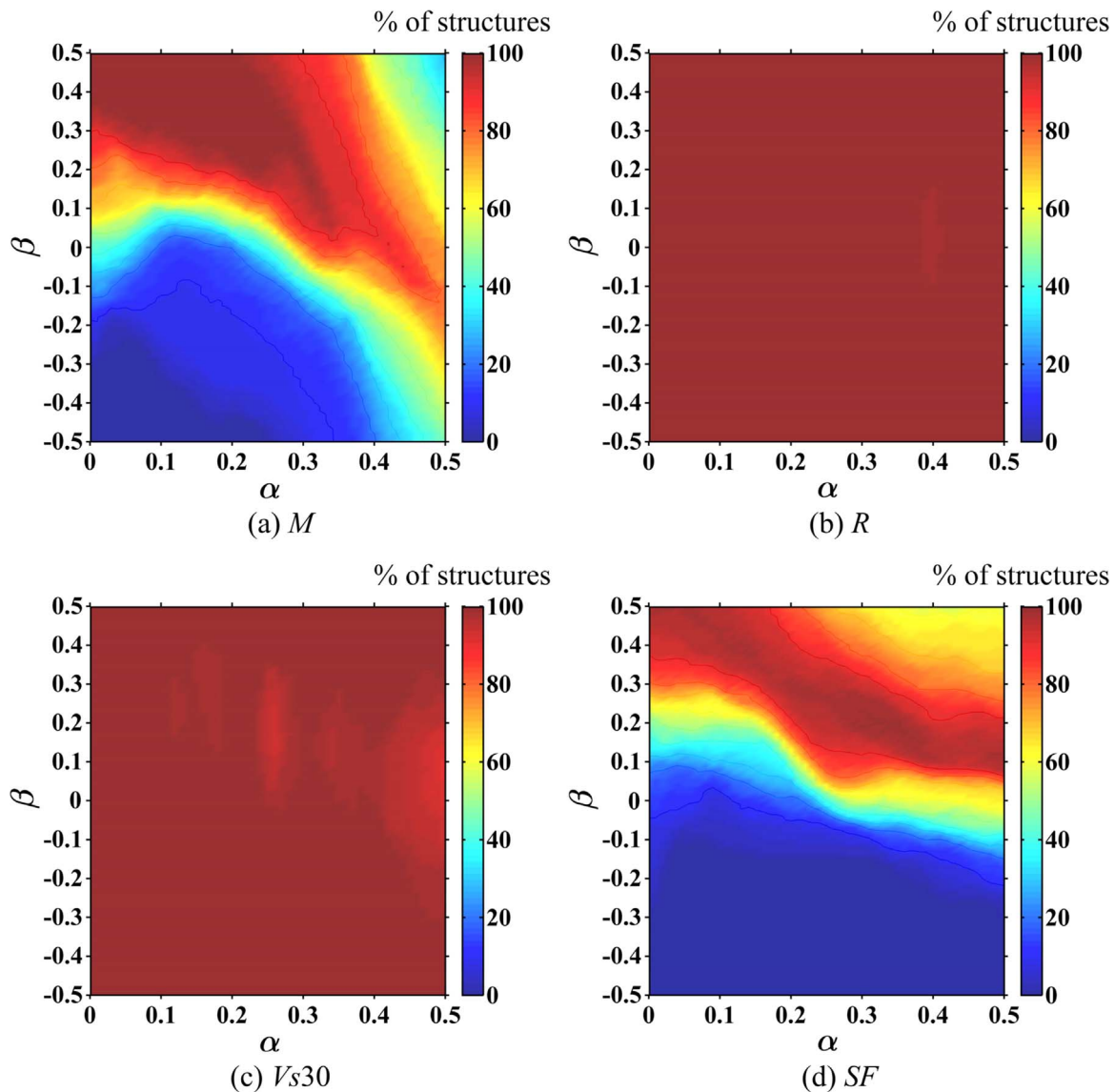
Fig. 7. Percent of structures with p-values ≥ 0.05 obtained from investigating the sufficiency of IM_{M-D} given $m = 0.5$, with respect to (a) M, (b) R, (c) $Vs30$ and (d) SF assuming different values of α and β.

for each of the IMs, this table presents the percent of structures with p-values ≥ 0.05 obtained from testing the sufficiency of IM with respect to each of these parameters. It can be seen that none of the IMs is simultaneously sufficient with respect to M, R, $Vs30$ and SF for all of the structures. It should be noted that $Sa(T_1)$, as the most common scalar IM, satisfies the sufficiency with respect to M and SF for 42.95% and 13.46% of the structures, respectively. The results show that I_v, which is the most efficient IM, satisfies the sufficiency with respect to M for only 30.13% of the structures, and does not satisfy the sufficiency with respect to SF for any of the structures. Moreover, a comparison between IM_M ($\alpha = 0.33$) and Sa_{avg} indicates that both the IMs are sufficient with respect to M for more than 80% of the structures, but their sufficiency with respect to SF is not comparable. In other words, IM_M ($\alpha = 0.33$) is sufficient with respect to SF for 53.85% of the structures, whereas Sa_{avg} is sufficient with respect to SF for 5.77% of the structures. Among the most efficient spectral shape based IMs, the sufficiency of IM_M ($\alpha = 0.5$) with respect to SF is higher than those of IM_M ($\alpha = 0.33$) and Sa_{avg}, but its sufficiency with respect to M is lower than those of IM_M ($\alpha = 0.33$) and Sa_{avg}.

In summary, it seems that the most efficient IMs presented in Table 4 are facing the sufficiency problems with respect to either M or

SF (or both). Thus, considering the effect of ground motion duration in the combined spectral shape and duration based IMs may improve the sufficiency of these IMs, when compared with the spectral shape based IMs. Fig. 6(a)–(c) show the results from investigating the sufficiency of the three IMs considered in Fig. 4 (i.e., IM_{C-D}, I_{Np-D} and Sa_{avg-D}) with respect to M, $Vs30$ and SF, respectively, as functions of β. Due to the fact that given all values of β, these IMs are sufficient with respect to R for more than 99% of the structures, the results of testing the sufficiency of the IMs with respect to R are not presented in this figure. It should be noted that when β is zero, IM_{C-D}, I_{Np-D} and Sa_{avg-D} are simplified to IM_C, I_{Np} and Sa_{avg}, respectively. Fig. 6(a) shows that as the value of β varies from -0.5 to 0.2, the sufficiency of IM_{C-D}, I_{Np-D} and Sa_{avg-D} with respect to M is significantly improved. Fig. 6(b) shows that the variation of β does not have a considerable effect on the sufficiency of the IMs with respect to $Vs30$. Fig. 6(c) shows that as the value of β varies from -0.5 to 0.3, the sufficiency of the IMs with respect to SF is significantly improved.

According to the results of the sensitivity analyses performed to investigate the effects of the value considered for β on the efficiency and sufficiency of the IMs IM_{C-D}, I_{Np-D} and Sa_{avg-D}, the optimal values of β equal to 0.2, 0.3 and 0.3 were selected for use in these IMs, respectively.
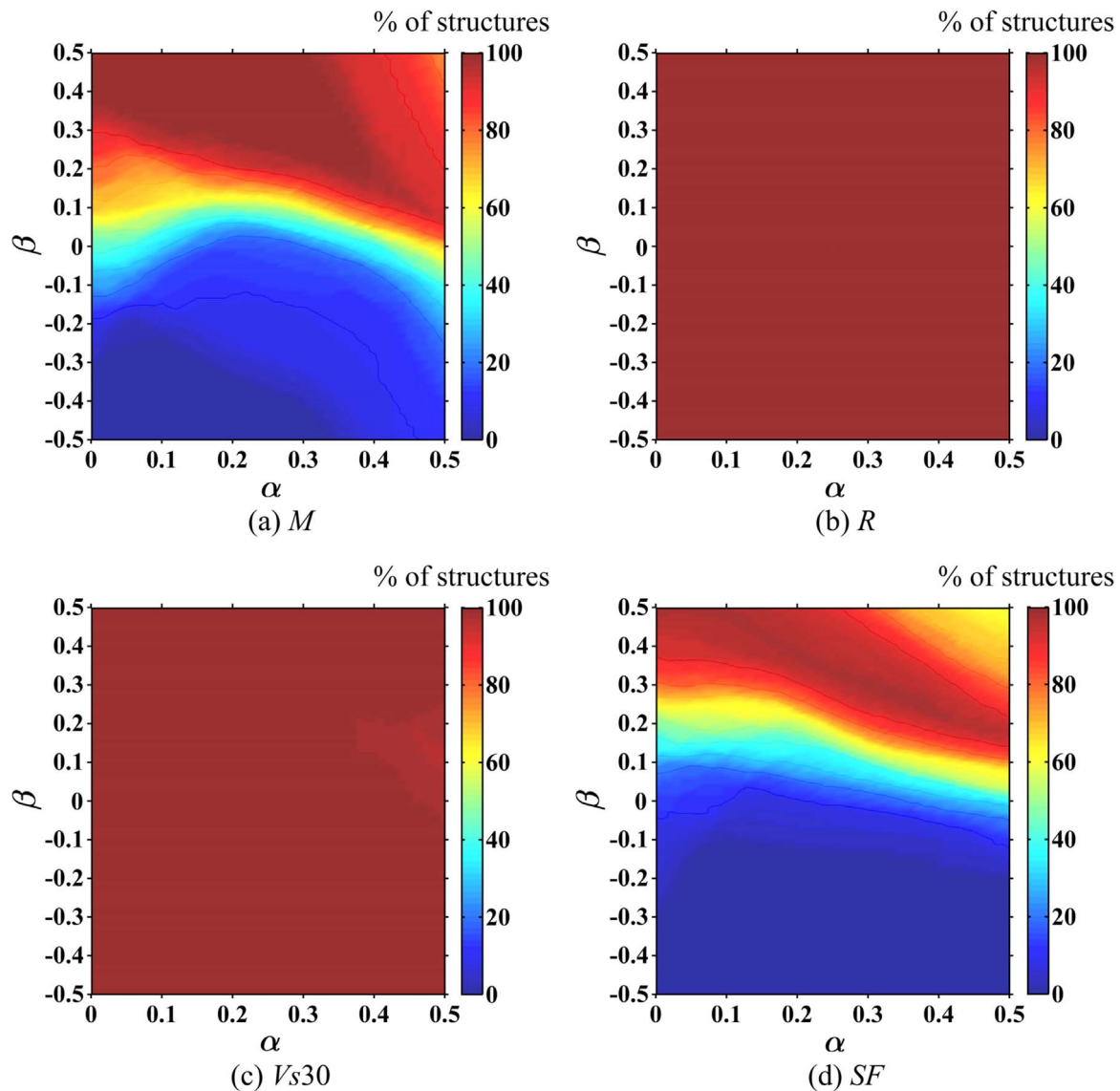
Fig. 8. Percent of structures with p-values ≥ 0.05 obtained from investigating the sufficiency of $I_{Np\ M-D}$ given $n = 0.6$, with respect to (a) M, (b) R, (c) $Vs30$ and (d) SF assuming different values of α and β.

In other words, using the selected optimal values of β for the three IMs, which were obtained by considering both the efficiency and sufficiency criteria, leads to more reliable results, when compared with the other values of β.

Fig. 7(a)–(d) show the results from investigating the sufficiency of IM_{M-D} given $m = 0.5$, with respect to M, R, $Vs30$ and SF, respectively, assuming different values of α and β. The contours in each of these figures illustrate the percent of structures with p-values ≥ 0.05 obtained considering one of the aforementioned parameters. In regard to these figures, using the points (α, β) corresponding to the dark red regions for IM_{M-D} leads to considerable sufficiency for this IM. To select the optimal values of α and β for use in IM_{M-D}, Figs. 5(a) and 7 should be simultaneously considered, and a point (α, β) corresponding to high efficiency and also acceptable sufficiency should be found. According to these figures, the point $(\alpha = 0.3, \beta = 0.2)$ was selected as an optimal point for use in IM_{M-D}.

Fig. 8(a)–(d) show the results from investigating the sufficiency of $I_{Np\ M-D}$ given $n = 0.6$, with respect to M, R, $Vs30$ and SF, respectively, assuming different values of α and β. According to Figs. 5(b) and 8, the point $(\alpha = 0.4, \beta = 0.2)$ was selected as an optimal point for use in $I_{Np\ M-D}$, by a method similar to that applied for IM_{M-D}.

Fig. 9(a)–(d) show the results from investigating the sufficiency of $Sa_{avg\ M-D}$ given $c_1 = 0.6$, with respect to M, R, $Vs30$ and SF, respectively, assuming different values of α and β. According to Figs. 5(c) and 9, the point $(\alpha = 0.4, \beta = 0.1)$ was selected as an optimal point for use in $Sa_{avg\ M-D}$, by a method similar to those applied for IM_{M-D} and $I_{Np\ M-D}$.

6. Proposing optimal IMs

As mentioned previously, the most efficient IMs considered in Table 4 are facing the sufficiency problems with respect to either M or SF (or both). In this section, the efficiency and sufficiency of the combined spectral shape and duration based IMs are investigated. Table 5 compares the efficiency and sufficiency of these IMs, given the selected optimal values of the parameters for these IMs. It can be seen that the first three IMs (i.e., IM_{C-D}, I_{Np-D} and Sa_{avg-D}) are less efficient than the other three IMs. Among the IMs IM_{M-D}, $I_{Np\ M-D}$ and $Sa_{avg\ M-D}$, $Sa_{avg\ M-D}$ is the most efficient one, but its sufficiency with respect to M and SF is lower than those of the other two IMs. Furthermore, IM_{M-D} is the most sufficient IM, but its efficiency is lower than those of the other two IMs. In summary, it can be inferred that using the IMs IM_{M-D}, $I_{Np\ M-D}$ and $Sa_{avg\ M-D}$ to predict the collapse capacity of the considered structures,
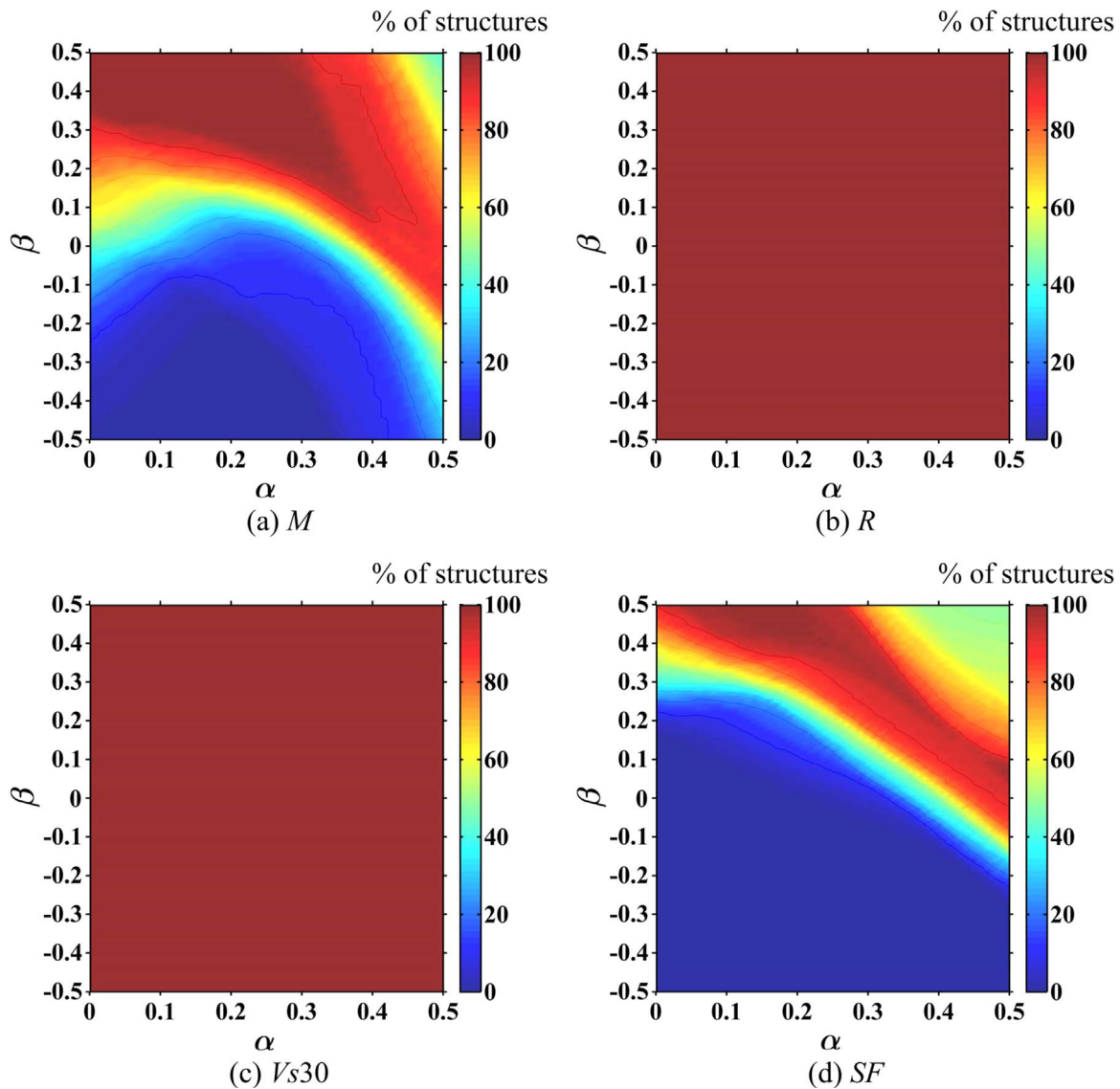
Fig. 9. Percent of structures with p-values ≥ 0.05 obtained from investigating the sufficiency of $Sa_{avg\ M-D}$ given $c_1 = 0.6$, with respect to (a) M, (b) R, (c) $Vs30$ and (d) SF assuming different values of α and β.

Table 5
Results from investigating the efficiency and sufficiency of the combined spectral shape and duration based IMs, given the selected optimal values of the parameters for these IMs.

IM	Mean value of dispersion, $(\sigma_{\ln IMcol})_{avg}$	Coefficient of variation for $\sigma_{\ln IMcol}$ values	% of structures with p-values ≥ 0.05			
			M	R	$Vs30$	SF
IM_{C-D} ($\beta = 0.2$)	0.300	0.1077	92.95	100	94.87	92.95
I_{Np-D} ($\beta = 0.3$)	0.315	0.1289	100	100	98.08	91.03
Sa_{avg-D} ($\beta = 0.3$)	0.287	0.0920	80.13	100	98.72	85.26
IM_{M-D} ($m = 0.5, \alpha = 0.3, \beta = 0.2$)	0.245	0.0717	98.72	100	99.36	98.08
$I_{Np\ M-D}$ ($n = 0.6, \alpha = 0.4, \beta = 0.2$)	0.230	0.0943	98.08	100	98.08	93.59
$Sa_{avg\ M-D}$ ($c_1 = 0.6, \alpha = 0.4, \beta = 0.1$)	0.187	0.0937	91.03	100	100	90.38

leads to more reliable results, when compared with the other IMs. Thus, these IMs are proposed as advanced scalar IMs to predict the collapse capacity of steel SMRFs equipped with FVDs. It should be noted that in the case of the SMRFs without FVDs, the proposed IMs have considerable efficiency and sufficiency so that their corresponding mean values of dispersion are approximately the same with those presented in Table 5 and they are sufficient for more than 90% of the SMRFs without FVDs.

Fig. 10 illustrates the fractional reductions in $(\sigma_{\ln IMcol})_{avg}$ achieved by the proposed IMs with respect to $Sa(T_1)$ and three well-known spectral shape based IMs (i.e., IM_C, I_{Np} and Sa_{avg}). Each bar in this figure represents the fractional reduction in $(\sigma_{\ln IMcol})_{avg}$ achieved by one of the proposed IMs with respect to one of the four above-mentioned IMs. It can be seen that the largest fractional reduction in $(\sigma_{\ln IMcol})_{avg}$ is 51.61%, which is achieved by $Sa_{avg\ M-D}$ with respect to $Sa(T_1)$. Furthermore, the smallest fractional reduction in $(\sigma_{\ln IMcol})_{avg}$ achieved by $Sa_{avg\ M-D}$ is with respect to Sa_{avg}.

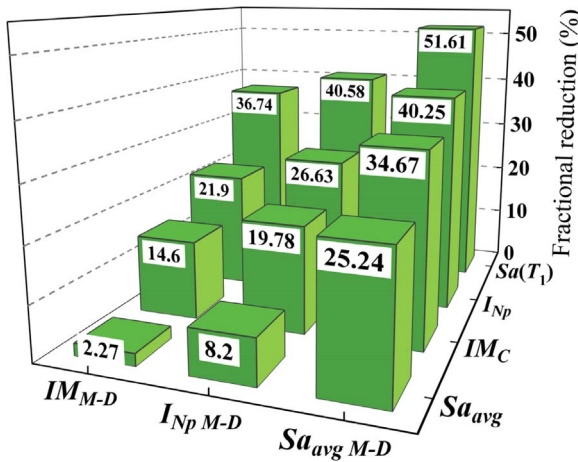Fig. 11(a)–(d) illustrate the amounts of increase in number of

Fig. 10. Fractional reductions in $(\sigma_{\ln IMcol})_{avg}$ achieved by the proposed IMs with respect to $Sa(T_1)$ and three well-known spectral shape based IMs.

structures with p-values $\geq$ 0.05 normalized to the total number of structures (in percent), calculated from comparing the sufficiency of the proposed IMs, with respect to M and SF, with those of the IMs $Sa(T_1)$, IM_C, I_{Np} and Sa_{avg}, respectively. It can be seen that the proposed IMs possess significantly higher sufficiency with respect to SF, when compared with $Sa(T_1)$, IM_C, I_{Np} and Sa_{avg}. Furthermore, in the case of sufficiency with respect to M, the proposed IMs possess higher sufficiency

compared with the four considered IMs, particularly I_{Np} and $Sa(T_1)$ that have low sufficiency with respect to M.

Table 6 presents the values of $\sigma_{\ln IMcol}$ obtained for the 156 structures considered in this study using the three proposed IMs. It can be seen that when the damping ratio of a structure increases, the corresponding $\sigma_{\ln IMcol}$ does not necessarily increase. Fig. 12 indicates the collapse fragility curves developed by using the three proposed IMs and seven other scalar IMs for the 3-, 6- and 9-story structures with linear FVDs and a supplemental viscous damping ratio of 0.1. To develop the collapse fragility curves using different IMs, the distributions of IM_{col} values were assumed to be lognormal. Moreover, to compare the collapse fragility curves, the values of IM_{col} obtained using each IM were normalized to their corresponding median collapse capacity, which is the exponential of the mean of the $\ln IM_{col}$ values. It can be seen that for the three structures considered, the collapse fragility curves corresponding to the proposed IMs are steeper than the other ones. This is because of the fact that these IMs are more efficient than the other IMs, and thus their corresponding $\sigma_{\ln IMcol}$ values are lower than those of the other IMs. It should be mentioned that the same observations hold true for all the structures considered in this study, but due to space limitation, collapse fragility curves are only presented for the three aforementioned structures.

As described previously, one of the desirable features of an optimal IM is scaling robustness. Fig. 13 illustrates a comparison between the scaling robustness of three well-known spectral shape based IMs and the proposed IMs to predict the collapse capacity of the 6-story-h_{typ}1.2 structure with nonlinear FVDs, having α_d = 0.5, and a supplemental
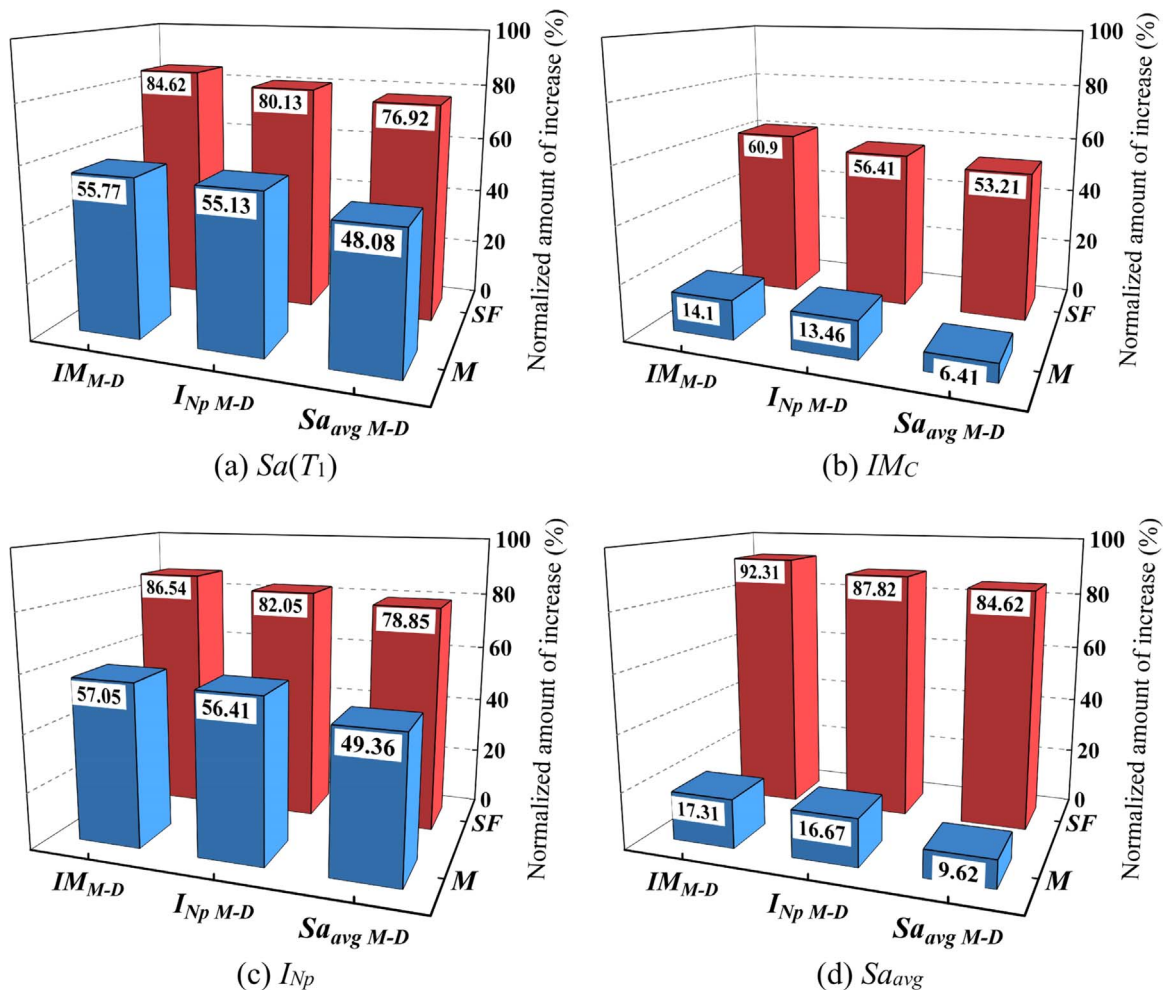

Fig. 11. Normalized amounts of increase in number of structures with p-values $\geq$ 0.05 (in percent) calculated from comparing the sufficiency of the proposed IMs, with respect to M and SF, with those of (a) $Sa(T_1)$, (b) IM_C, (c) I_{Np} and (d) Sa_{avg}.

Table 6
Values of $\sigma_{\ln IMcol}$ obtained for the 156 structures considered in this study using the three proposed IMs.

Structure	IM	α_d = 1.0	0.05				0.1				0.15				Average
			1.0	0.75	0.5	0.25	1.0	0.75	0.5	0.25	1.0	0.75	0.5	0.25	
3-story	A	0.233	0.234	0.230	0.222	0.220	0.230	0.230	0.228	0.215	0.250	0.229	0.222	0.218	0.228
	B	0.206	0.208	0.204	0.200	0.199	0.207	0.206	0.207	0.201	0.227	0.204	0.205	0.208	0.206
	C	0.188	0.183	0.177	0.175	0.174	0.185	0.178	0.170	0.172	0.207	0.179	0.174	0.166	0.179
3-story-h1.2	A	0.245	0.229	0.232	0.236	0.243	0.241	0.241	0.243	0.239	0.245	0.238	0.241	0.239	0.239
	B	0.221	0.211	0.214	0.218	0.222	0.225	0.223	0.226	0.222	0.230	0.220	0.225	0.223	0.222
	C	0.185	0.192	0.189	0.184	0.185	0.212	0.203	0.199	0.188	0.225	0.207	0.202	0.192	0.197
3-story-h1.4	A	0.247	0.224	0.236	0.238	0.243	0.230	0.240	0.236	0.245	0.234	0.239	0.241	0.247	0.238
	B	0.232	0.219	0.226	0.229	0.232	0.224	0.233	0.231	0.239	0.228	0.232	0.234	0.240	0.231
	C	0.193	0.186	0.192	0.189	0.190	0.194	0.201	0.193	0.196	0.200	0.199	0.196	0.194	0.194
3-story-$h_1$1.2	A	0.250	0.249	0.250	0.247	0.245	0.240	0.245	0.243	0.239	0.259	0.237	0.242	0.240	0.245
	B	0.214	0.215	0.216	0.214	0.215	0.213	0.214	0.214	0.214	0.232	0.209	0.214	0.220	0.216
	C	0.183	0.179	0.176	0.173	0.173	0.182	0.174	0.170	0.168	0.199	0.175	0.170	0.169	0.176
3-story-$h_1$1.4	A	0.223	0.223	0.222	0.214	0.217	0.232	0.232	0.230	0.232	0.256	0.240	0.237	0.234	0.230
	B	0.206	0.204	0.203	0.190	0.194	0.216	0.215	0.210	0.213	0.239	0.226	0.220	0.216	0.212
	C	0.178	0.183	0.176	0.167	0.167	0.202	0.194	0.184	0.183	0.224	0.207	0.196	0.186	0.188
3-story-m1.2	A	0.258	0.251	0.250	0.249	0.258	0.248	0.264	0.253	0.252	0.255	0.248	0.253	0.240	0.252
	B	0.226	0.218	0.217	0.219	0.227	0.220	0.232	0.223	0.225	0.231	0.220	0.225	0.220	0.223
	C	0.196	0.183	0.181	0.183	0.190	0.189	0.195	0.185	0.182	0.203	0.186	0.185	0.174	0.187
3-story-m1.4	A	0.250	0.233	0.236	0.235	0.239	0.239	0.239	0.243	0.243	0.250	0.242	0.245	0.247	0.242
	B	0.228	0.207	0.209	0.209	0.212	0.214	0.212	0.217	0.217	0.228	0.217	0.220	0.224	0.216
	C	0.179	0.172	0.172	0.168	0.168	0.181	0.176	0.179	0.177	0.199	0.182	0.182	0.183	0.178
6-story	A	0.225	0.252	0.228	0.228	0.230	0.274	0.245	0.241	0.237	0.284	0.257	0.249	0.246	0.246
	B	0.214	0.247	0.222	0.219	0.219	0.274	0.244	0.234	0.229	0.280	0.258	0.243	0.239	0.240
	C	0.190	0.213	0.195	0.192	0.191	0.237	0.214	0.204	0.199	0.245	0.231	0.215	0.207	0.210
6-story-h_{typ}1.2	A	0.246	0.247	0.236	0.233	0.233	0.258	0.238	0.246	0.233	0.270	0.243	0.234	0.232	0.242
	B	0.233	0.242	0.229	0.225	0.227	0.252	0.234	0.242	0.231	0.272	0.242	0.234	0.230	0.238
	C	0.184	0.192	0.182	0.178	0.179	0.204	0.186	0.189	0.181	0.222	0.196	0.187	0.180	0.189
6-story-h_{typ}1.4	A	0.249	0.237	0.239	0.241	0.242	0.249	0.254	0.242	0.242	0.264	0.258	0.248	0.245	0.247
	B	0.238	0.228	0.229	0.231	0.232	0.245	0.244	0.234	0.235	0.263	0.256	0.241	0.238	0.240
	C	0.172	0.165	0.162	0.162	0.162	0.181	0.174	0.163	0.162	0.198	0.188	0.166	0.171	0.171
9-story	A	0.240	0.241	0.233	0.234	0.231	0.253	0.235	0.230	0.228	0.292	0.246	0.235	0.234	0.241
	B	0.231	0.234	0.228	0.231	0.228	0.242	0.228	0.227	0.227	0.273	0.238	0.231	0.231	0.234
	C	0.168	0.177	0.168	0.167	0.162	0.183	0.157	0.157	0.156	0.207	0.164	0.152	0.150	0.167
9-story-h_{typ}1.2	A	0.283	0.297	0.275	0.284	0.286	0.290	0.299	0.285	0.278	0.295	0.287	0.297	0.289	0.288
	B	0.278	0.294	0.267	0.276	0.279	0.284	0.292	0.280	0.275	0.285	0.283	0.291	0.286	0.282
	C	0.210	0.221	0.202	0.209	0.207	0.221	0.218	0.202	0.196	0.223	0.215	0.211	0.199	0.210

A = IM_{M-D}, B = $I_{Np\ M-D}$, C = $Sa_{avg\ M-D}$

viscous damping ratio of 0.1. It can be seen than the proposed IMs possess high sufficiency with respect to SF, whereas the other IMs are insufficient with respect to SF.

7. GMPEs for the proposed IMs

As mentioned previously, one of the desirable features of an optimal IM is predictability. In fact, the predictability of the proposed IMs is crucial for the applicability of these IMs. The reason for this issue is that to perform Probabilistic Seismic Hazard Analysis (PSHA) using a proposed IM, a reliable GMPE for the IM is required. Other researchers [31,46,59–61] have presented GMPEs for some of the spectral shape based IMs considered in this study using the GMPE for $Sa(T)$ and correlation of spectral acceleration values. However, because the IMs proposed in this study are combined spectral shape and duration based IMs, to present GMPEs for these IMs, additional information is required. In this section, to satisfy the predictability criterion for the proposed IMs and facilitate their use for conducting PSHA, GMPEs are presented for these IMs. Assuming lognormal distribution for the proposed IMs, the logarithmic means and standard deviations of these IMs can be determined based on the GMPEs for $Sa(T)$ and t_d existing in the technical literature (e.g., the Campbell and Bozorgnia GMPE [62] for $Sa(T)$ and the GMPE proposed by Bommer et al. [63] for t_d). Moreover, correlation of spectral acceleration values and also correlation of significant duration with spectral acceleration values are required. To obtain these correlations, the empirical equations proposed by Baker and Jayaram [64] and Bradley [65] can be used.

The logarithmic mean and standard deviation of IM_{M-D} can be obtained, respectively, as follows:

$$E(\ln IM_{M-D}) = (1-m)\,E(\ln Sa(T_1)) + m\,E(\ln Sa(R^\alpha T_1)) + \beta\,E(\ln t_d) \tag{10}$$

$$
\begin{aligned}
\sigma_{\ln IM_{M-D}} = \ & \big((1-m)^2\sigma^2_{\ln Sa(T_1)} + m^2\sigma^2_{\ln Sa(R^\alpha T_1)} \\
& + \beta^2\sigma^2_{\ln t_d} + 2m(1-m)\rho_{\ln Sa(T_1),\,\ln Sa(R^\alpha T_1)} \\
& \times \sigma_{\ln Sa(T_1)}\sigma_{\ln Sa(R^\alpha T_1)} + 2\beta(1-m)\,\rho_{\ln Sa(T_1),\,\ln t_d} \\
& \times \sigma_{\ln Sa(T_1)}\sigma_{\ln t_d} + 2\beta m\,\rho_{\ln Sa(R^\alpha T_1),\,\ln t_d} \\
& \times \sigma_{\ln Sa(R^\alpha T_1)}\sigma_{\ln t_d}\big)^{0.5}
\end{aligned}
\tag{11}
$$

where $E(\ln Sa(T_1))$, $E(\ln Sa(R^\alpha T_1))$ and $E(\ln t_d)$ are the logarithmic means of $Sa(T_1)$, $Sa(R^\alpha T_1)$ and t_d, respectively; $\sigma_{\ln Sa(T_1)}$, $\sigma_{\ln Sa(R^\alpha T_1)}$ and $\sigma_{\ln t_d}$ are the logarithmic standard deviations of $Sa(T_1)$, $Sa(R^\alpha T_1)$ and t_d, respectively; and $\rho_{\ln Sa(T_1),\,\ln Sa(R^\alpha T_1)}$, $\rho_{\ln Sa(T_1),\,\ln t_d}$ and $\rho_{\ln Sa(R^\alpha T_1),\,\ln t_d}$ are the correlations of $\ln Sa(T_1)$ and $\ln Sa(R^\alpha T_1)$, $\ln Sa(T_1)$ and $\ln t_d$, and $\ln Sa(R^\alpha T_1)$ and $\ln t_d$, respectively. $\rho_{\ln Sa(T_1),\,\ln Sa(R^\alpha T_1)}$ can be obtained using the equation proposed by Baker and Jayaram [64], whereas $\rho_{\ln Sa(T_1),\,\ln t_d}$ and $\rho_{\ln Sa(R^\alpha T_1),\,\ln t_d}$ can be obtained using the equation proposed by Bradley [65].

The logarithmic mean and standard deviation of $I_{Np\ M-D}$ can be obtained, respectively, as follows:
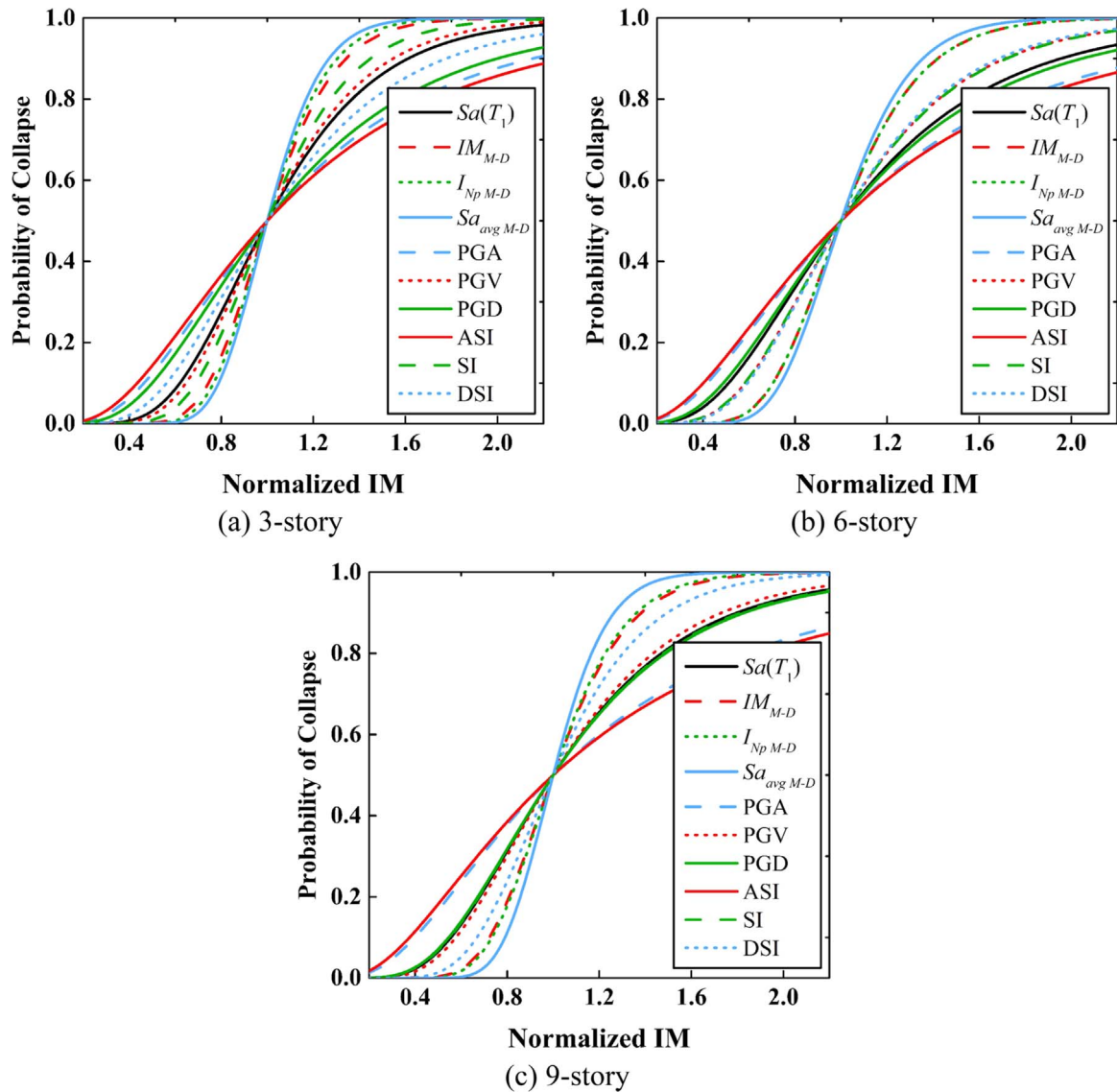
Fig. 12. Collapse fragility curves developed by using different IMs for the 3-, 6- and 9-story structures with linear FVDs and a supplemental viscous damping ratio of 0.1.

$$E(\ln I_{Np\,M-D}) = (1-n)\,E(\ln Sa\,(T_1)) + \frac{n}{N}\sum_{i=1}^{N} E(\ln Sa\,(T_i)) + \beta\,E(\ln t_d) \tag{12}$$

$$\begin{aligned}\sigma_{\ln I_{Np\,M-D}} = &\,((1-n)^2\sigma_{\ln Sa(T_1)}^2 + n^2\sigma_{\ln Sa_{avg}(T_1\ldots T_N)}^2\\ &+ \beta^2\sigma_{\ln t_d}^2 + 2n(1-n)\rho_{\ln Sa(T_1),\,\ln Sa_{avg}(T_1\ldots T_N)}\\ &\times\,\sigma_{\ln Sa(T_1)}\sigma_{\ln Sa_{avg}(T_1\ldots T_N)} + 2\beta(1-n)\rho_{\ln Sa(T_1),\,\ln t_d}\\ &\times\,\sigma_{\ln Sa(T_1)}\sigma_{\ln t_d} + 2\beta n\rho_{\ln Sa_{avg}(T_1\ldots T_N),\,\ln t_d}\\ &\times\,\sigma_{\ln Sa_{avg}(T_1\ldots T_N)}\sigma_{\ln t_d})^{0.5}\end{aligned} \tag{13}$$

where $E(\ln Sa(T_i))$ is the logarithmic mean of $Sa(T_i)$, $\sigma_{\ln Sa_{avg}(T_1\ldots T_N)}$ is the logarithmic standard deviation of $Sa_{avg}(T_1\ldots T_N)$; and $\rho_{\ln Sa(T_1),\,\ln Sa_{avg}(T_1\ldots T_N)}$ and $\rho_{\ln Sa_{avg}(T_1\ldots T_N),\,\ln t_d}$ are the correlations of $\ln Sa$ (T_1) and $\ln Sa_{avg}(T_1\ldots T_N)$, and $\ln Sa_{avg}(T_1\ldots T_N)$ and $\ln t_d$, respectively. $\sigma_{\ln Sa_{avg}(T_1\ldots T_N)}$, $\rho_{\ln Sa(T_1),\,\ln Sa_{avg}(T_1\ldots T_N)}$ and $\rho_{\ln Sa_{avg}(T_1\ldots T_N),\,\ln t_d}$ can be obtained using the following equations:

$$\sigma_{\ln Sa_{avg}(T_1\ldots T_N)} = \left(\frac{1}{N^2}\sum_{i=1}^{N}\sum_{j=1}^{N}\rho_{\ln Sa(T_i),\,\ln Sa(T_j)}\sigma_{\ln Sa(T_i)}\sigma_{\ln Sa(T_j)}\right)^{0.5} \tag{14}$$

$$\rho_{\ln Sa(T_1),\,\ln Sa_{avg}(T_1\ldots T_N)} = \frac{\sum_{i=1}^{N}\rho_{\ln Sa(T_1),\,\ln Sa(T_i)}\sigma_{\ln Sa(T_i)}}{\sqrt{\sum_{i=1}^{N}\sum_{j=1}^{N}\rho_{\ln Sa(T_i),\,\ln Sa(T_j)}\sigma_{\ln Sa(T_i)}\sigma_{\ln Sa(T_j)}}} \tag{15}$$

$$\rho_{\ln Sa_{avg}(T_1\ldots T_N),\,\ln t_d} = \frac{\sum_{i=1}^{N}\rho_{\ln t_d,\,\ln Sa(T_i)}\sigma_{\ln Sa(T_i)}}{\sqrt{\sum_{i=1}^{N}\sum_{j=1}^{N}\rho_{\ln Sa(T_i),\,\ln Sa(T_j)}\sigma_{\ln Sa(T_i)}\sigma_{\ln Sa(T_j)}}} \tag{16}$$

where $\sigma_{\ln Sa(T_i)}$ and $\sigma_{\ln Sa(T_j)}$ are the logarithmic standard deviations of Sa (T_i) and $Sa(T_j)$, respectively; $\rho_{\ln Sa(T_i),\,\ln Sa(T_j)}$ and $\rho_{\ln Sa(T_1),\,\ln Sa(T_i)}$ are the correlations of $\ln Sa(T_i)$ and $\ln Sa(T_j)$, and $\ln Sa(T_1)$ and $\ln Sa(T_i)$, respectively, which can be obtained using the equation proposed by Baker and Jayaram [64]; and $\rho_{\ln t_d,\,\ln Sa(T_i)}$ is the correlation of $\ln t_d$ and $\ln Sa$ (T_i), which can be obtained using the equation proposed by Bradley [65].

The logarithmic mean and standard deviation of $Sa_{avg\,M-D}$ can be obtained, respectively, as follows:

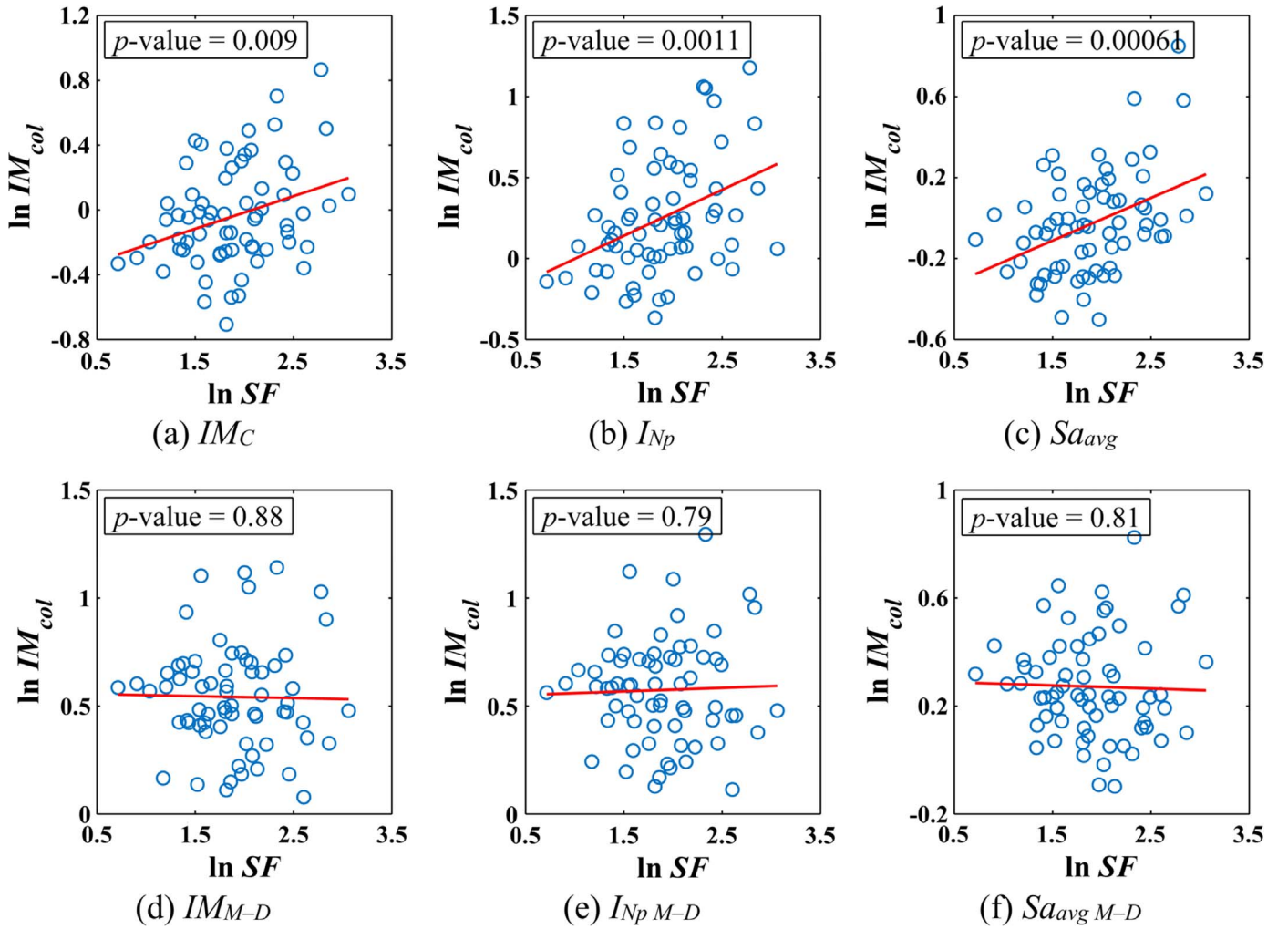$$E(\ln Sa_{avg\,M-D}) = \frac{1}{N}\sum_{i=1}^{N} E(\ln Sa(c_i T_1)) + \beta E(\ln t_d) \tag{17}$$

Fig. 13. Comparison between the scaling robustness of (a) IM_C, (b) I_{Np}, (c) Sa_{avg}, (d) IM_{M-D}, (e) $I_{Np\ M-D}$ and (f) $Sa_{avg\ M-D}$ to predict the collapse capacity of the 6-story-h_{typ}1.2 structure with nonlinear FVDs, having $\alpha_d = 0.5$, and $\xi_v = 0.1$.

$$\sigma_{\ln Sa_{avg\ M-D}} = (\sigma^2_{\ln Sa_{avg}(c_1 T_1...c_N T_1)} + \beta^2 \sigma^2_{\ln t_d} + 2\beta \rho_{\ln Sa_{avg}(c_1 T_1...c_N T_1),\ \ln t_d}$$
$$\times \sigma_{\ln Sa_{avg}(c_1 T_1...c_N T_1)} \sigma_{\ln t_d})^{0.5}$$

(18)

where $E(\ln Sa(c_i T_1))$ is the logarithmic mean of $Sa(c_i T_1)$, $\sigma_{\ln Sa_{avg}(c_1 T_1...c_N T_1)}$ is the logarithmic standard deviation of $Sa_{avg}(c_1 T_1...c_N T_1)$, and $\rho_{\ln Sa_{avg}(c_1 T_1...c_N T_1),\ \ln t_d}$ is the correlation of $\ln Sa_{avg}(c_1 T_1...c_N T_1)$ and $\ln t_d$. $\sigma_{\ln Sa_{avg}(c_1 T_1...c_N T_1)}$ and $\rho_{\ln Sa_{avg}(c_1 T_1...c_N T_1),\ \ln t_d}$ can be obtained using the following equations:

$$\sigma_{\ln Sa_{avg}(c_1 T_1...c_N T_1)} = \left(\frac{1}{N^2} \sum_{i=1}^{N} \sum_{j=1}^{N} \rho_{\ln Sa(c_i T_1),\ \ln Sa(c_j T_1)} \sigma_{\ln Sa(c_i T_1)} \sigma_{\ln Sa(c_j T_1)}\right)^{0.5}$$

(19)

$$\rho_{\ln Sa_{avg}(c_1 T_1...c_N T_1),\ \ln t_d} = \frac{\sum_{i=1}^{N} \rho_{\ln t_d,\ \ln Sa(c_i T_1)} \sigma_{\ln Sa(c_i T_1)}}{\sqrt{\sum_{i=1}^{N} \sum_{j=1}^{N} \rho_{\ln Sa(c_i T_1),\ \ln Sa(c_j T_1)} \sigma_{\ln Sa(c_i T_1)} \sigma_{\ln Sa(c_j T_1)}}}$$

(20)

where $\sigma_{\ln Sa(c_i T_1)}$ and $\sigma_{\ln Sa(c_j T_1)}$ are the logarithmic standard deviations of $Sa(c_i T_1)$ and $Sa(c_j T_1)$, respectively; and $\rho_{\ln Sa(c_i T_1),\ \ln Sa(c_j T_1)}$ and $\rho_{\ln t_d,\ \ln Sa(c_i T_1)}$ are the correlations of $\ln Sa(c_i T_1)$ and $\ln Sa(c_j T_1)$, and $\ln t_d$ and $\ln Sa(c_i T_1)$, respectively.

8. Conclusions

In this study, the efficiency and sufficiency of 27 scalar IMs, including 13 non-structure-specific and 14 structure-specific IMs, to predict the collapse capacity of steel SMRFs with and without FVDs were investigated. For this purpose, 12 SMRF structures including three code-designed benchmark structures and nine structures derived from the benchmark structures, by changing their height or seismic mass, were considered. In addition to the 12 SMRF structures, assuming three levels of supplemental viscous damping ratio, linear and nonlinear FVDs were added to the SMRFs and 144 SMRFs with FVDs were considered. The obtained results indicated that none of the non-structure-specific IMs could satisfy both the efficiency and sufficiency criteria. The structure-specific IMs consist of $Sa(T_1)$, the spectral shape based IMs and the combined spectral shape and duration based IMs. It was indicated that among the spectral shape based IMs, IM_C, I_{Np}, IM_M and Sa_{avg} are more efficient than the others, but they are facing the sufficiency problems with respect to either M or SF (or both). The combined spectral shape and duration based IMs are IM_{C-D}, IM_{M-D}, I_{Np-D}, $I_{Np\ M-D}$, Sa_{avg-D} and $Sa_{avg\ M-D}$. Sensitivity analyses were performed to select the optimal values of the parameters for these IMs by considering the efficiency and sufficiency criteria simultaneously. After selecting the optimal values of the parameters for use in the combined spectral shape and duration based IMs, the results obtained by using these IMs were compared, and the IMs IM_{M-D}, $I_{Np\ M-D}$ and $Sa_{avg\ M-D}$ were proposed as advanced scalar IMs to reliably predict the collapse capacity of steel

SMRFs with FVDs.

According to the results, the values of $(\sigma_{\ln IMcol})_{avg}$ obtained using $IM_{M–D}$, $I_{Np\ M–D}$ and $Sa_{avg\ M–D}$ are 0.24, 0.23 and 0.19, respectively. Thus, $Sa_{avg\ M–D}$ is more efficient than the other proposed IMs. Comparing the values of $(\sigma_{\ln IMcol})_{avg}$ obtained using the proposed IMs with that obtained using $Sa(T_1)$, which is 0.39, indicates the high efficiency of the proposed IMs. Moreover, the proposed IMs possess high sufficiency with respect to M and SF, when compared with the other IMs considered in this study. In other words, $IM_{M–D}$, $I_{Np\ M–D}$ and $Sa_{avg\ M–D}$ are sufficient with respect to M for 98.72%, 98.08% and 91.03% of the structures, respectively, and in the case of sufficiency with respect to SF, these IMs are sufficient for 98.08%, 93.59% and 90.38% of the structures, respectively. Therefore, it can be concluded that accounting for the effect of ground motion duration in the proposed IMs leads to high sufficiency with respect to M and SF for these IMs. Consequently, by using the proposed IMs, the collapse capacity of steel SMRFs with FVDs can be predicted more realistically. Furthermore, in the case of steel SMRFs without FVDs, the proposed IMs are also better than the other IMs. To satisfy the predictability criterion for the proposed IMs, GMPEs were presented for these IMs.

References

[1] Soong TT, Dargush GF. Passive energy dissipation systems in structural engineering. Chichester: Wiley; 1997.

[2] Constantinou MC, Soong TT, Dargush GF. Passive energy dissipation systems for structural design and retrofit [Monograph No. MCEER-98-MN01]. Buffalo, NY: Multidisciplinary Center for Earthquake Engineering Research; 1998.

[3] Symans MD, Charney FA, Whittaker AS, Constantinou MC, Kircher CA, Johnson MW, McNamara RJ. Energy dissipation systems for seismic applications: current practice and recent developments. J Struct Eng 2008;134(1):3–21. http://dx.doi.org/10.1061/(ASCE)0733-9445(2008)134:1(3).

[4] Landi L, Lucchi S, Diotallevi PP. A procedure for the direct determination of the required supplemental damping for the seismic retrofit with viscous dampers. Eng Struct 2014;71:137–49. http://dx.doi.org/10.1016/j.engstruct.2014.04.025.

[5] Chopra AK. Dynamics of structures: theory and applications to earthquake engineering. Fourth edition Upper Saddle River, NJ: Prentice Hall; 2012.

[6] Lin WH, Chopra AK. Earthquake response of elastic single-degree-of-freedom systems with nonlinear viscoelastic dampers. J Eng Mech 2003;129(6):597–606. http://dx.doi.org/10.1061/(ASCE)0733-9399(2003)129:6(597).

[7] Karavasilis TL, Seo CY. Seismic structural and non-structural performance evaluation of highly damped self-centering and conventional systems. Eng Struct 2011;33(8):2248–58. http://dx.doi.org/10.1016/j.engstruct.2011.04.001.

[8] Christopoulos C, Filiatrault A. Principles of passive supplemental damping and seismic isolation. Pavia: IUSS Press; 2006.

[9] Dong B, Sause R, Ricles JM. Seismic response and performance of a steel MRF building with nonlinear viscous dampers under DBE and MCE. J Struct Eng 2016;142(6):04016023. http://dx.doi.org/10.1061/(ASCE)ST.1943-541X.0001482.

[10] Palermo M, Silvestri S, Trombetti T. On the peak inter-storey drift and peak inter-storey velocity profiles for frame structures. Soil Dyn Earthq Eng 2017;94:18–34. http://dx.doi.org/10.1016/j.soildyn.2016.12.009.

[11] Ramirez OM, Constantinou MC, Kircher CA, Whittaker AS, Johnson MW, Gomez JD, Chrysostomou CZ. Development and evaluation of simplified procedures for analysis and design of buildings with passive energy dissipation systems [Report No. MCEER-00-0010 Revision 1]. Buffalo, NY: Multidisciplinary Center for Earthquake Engineering Research; 2001.

[12] Hwang JS, Huang YN, Yi SL, Ho SY. Design formulations for supplemental viscous dampers to building structures. J Struct Eng 2008;134(1):22–31. http://dx.doi.org/10.1061/(ASCE)0733-9445(2008)134:1(22).

[13] Silvestri S, Gasparini G, Trombetti T. A five-step procedure for the dimensioning of viscous dampers to be inserted in building structures. J Earthq Eng 2010;14(3):417–47. http://dx.doi.org/10.1080/13632460903093891.

[14] Vamvatsikos D, Cornell CA. Incremental dynamic analysis. Earthq Eng Struct Dyn 2002;31(3):491–514. http://dx.doi.org/10.1002/eqe.141.

[15] Ibarra LF, Krawinkler H. Global collapse of frame structures under seismic excitations [Report No. 152]. Stanford, CA: The John A. Blume Earthquake Engineering Research Center, Department of Civil Engineering, Stanford University; 2005.

[16] Haselton CB. Assessing collapse safety of modern reinforced concrete moment frame buildings [Ph.D. Dissertation]. Stanford, CA: Department of Civil and Environmental Engineering, Stanford University; 2006.

[17] ATC. Quantification of building seismic performance factors [FEMA P695 Report]. Redwood City, CA: Applied Technology Council; 2009.

[18] Hamidia M, Filiatrault A, Aref A. Simplified seismic collapse capacity-based evaluation and design of frame buildings with and without supplemental damping systems [Report No. MCEER-14-0001]. Buffalo, NY: Multidisciplinary Center for Earthquake Engineering Research; 2014.

[19] Seo CY, Karavasilis TL, Ricles JM, Sause R. Seismic performance and probabilistic collapse resistance assessment of steel moment resisting frames with fluid viscous dampers. Earthq Eng Struct Dyn 2014;43(14):2135–54. http://dx.doi.org/10.1002/eqe.2440.

[20] Karavasilis TL. Assessment of capacity design of columns in steel moment resisting frames with viscous dampers. Soil Dyn Earthq Eng 2016;88:215–22. http://dx.doi.org/10.1016/j.soildyn.2016.06.006.

[21] Luco N, Cornell CA. Structure-specific scalar intensity measures for near-source and ordinary earthquake ground motions. Earthq Spectra 2007;23(2):357–92. http://dx.doi.org/10.1193/1.2723158.

[22] Vamvatsikos D, Cornell CA. Developing efficient scalar and vector intensity measures for IDA capacity estimation by incorporating elastic spectral shape information. Earthq Eng Struct Dyn 2005;34(13):1573–600. http://dx.doi.org/10.1002/eqe.496.

[23] Bradley BA, Dhakal RP, MacRae GA, Cubrinovski M. Prediction of spatially distributed seismic demands in specific structures: ground motion and structural response. Earthq Eng Struct Dyn 2010;39(5):501–20. http://dx.doi.org/10.1002/eqe.954.

[24] Yakhchalian M, Nicknam A, Ghodrati Amiri G. Optimal vector-valued intensity measure for seismic collapse assessment of structures. Earthq Eng Eng Vib 2015;14(1):37–54. http://dx.doi.org/10.1007/s11803-015-0005-6.

[25] Bojórquez E, Iervolino I, Reyes-Salazar A, Ruiz SE. Comparing vector-valued intensity measures for fragility analysis of steel frames in the case of narrow-band ground motions. Eng Struct 2012;45:472–80. http://dx.doi.org/10.1016/j.engstruct.2012.07.002.

[26] Baker JW, Cornell CA. Vector-valued intensity measures for pulse-like near-fault ground motions. Eng Struct 2008;30(4):1048–57. http://dx.doi.org/10.1016/j.engstruct.2007.07.009.

[27] Shome N, Cornell CA, Bazzurro P, Carballo JE. Earthquakes, records, and nonlinear responses. Earthq Spectra 1998;14(3):469–500. http://dx.doi.org/10.1193/1.1586011.

[28] Cordova PP, Deierlein GG, Mehanny SSF, Cornell CA. Development of a two-parameter seismic intensity measure and probabilistic assessment procedure. In: Proceedings of The Second U.S.–Japan Workshop on Performance-Based Earthquake Engineering Methodology for Reinforced Concrete Building Structures, Sapporo, Hokkaido, Japan, 2000, p. 187–206.

[29] Mehanny SS. A broad-range power-law form scalar-based seismic intensity measure. Eng Struct 2009;31(7):1354–68. http://dx.doi.org/10.1016/j.engstruct.2009.02.003.

[30] Baker JW. Vector-valued ground motion intensity measures for probabilistic seismic demand analysis [Ph.D. dissertation]. Stanford, CA: Department of Civil and Environmental Engineering, Stanford University; 2005.

[31] Bojórquez E, Iervolino I. Spectral shape proxies and nonlinear structural response. Soil Dyn Earthq Eng 2011;31(7):996–1008. http://dx.doi.org/10.1016/j.soildyn.2011.03.006.

[32] Donaire-Ávila J, Mollaioli F, Lucchini A, Benavent-Climent A. Intensity measures for the seismic response prediction of mid-rise buildings with hysteretic dampers. Eng Struct 2015;102:278–95. http://dx.doi.org/10.1016/j.engstruct.2015.08.023.

[33] Yakhchalian M, Nicknam A, Ghodrati Amiri G. Proposing an optimal integral-based intensity measure for seismic collapse capacity assessment of structures under pulse-like near-fault ground motions. J Vibroeng 2014;16(3):1360–75.

[34] Eads L, Miranda E, Lignos DG. Average spectral acceleration as an intensity measure for collapse risk assessment. Earthq Eng Struct Dyn 2015;44(12):2057–73. http://dx.doi.org/10.1002/eqe.2575.

[35] Eads L, Miranda E, Lignos D. Spectral shape metrics and structural collapse potential. Earthq Eng Struct Dyn 2016;45(10):1643–59. http://dx.doi.org/10.1002/eqe.2739.

[36] Chandramohan R, Baker JW, Deierlein GG. Quantifying the influence of ground motion duration on structural collapse capacity using spectrally equivalent records. Earthq Spectra 2015;32(2). http://dx.doi.org/10.1193/122813EQS.298MR2. [927–50].

[37] Arias A. Hansen R, editor. A Measure of Earthquake Intensity. Seismic Design of Nuclear Power Plants. Cambridge, MA: MIT Press; 1970. p. 438–83.

[38] Park YJ, Ang AHS, Wen YK. Seismic damage analysis of reinforced concrete buildings. J Struct Eng 1985;111(4):740–57. http://dx.doi.org/10.1061/(ASCE)0733-9445(1985)111:4(740).

[39] Riddell R, Garcia J. Hysteretic energy spectrum and damage control. Earthq Eng Struct Dyn 2001;30(12):1791–816. http://dx.doi.org/10.1002/eqe.93.

[40] EPRI. A criterion for determining exceedance of the operating basis earthquake [Report NP-5930]. Palo Alto, CA: Electric Power Research Institute; 1988.

[41] Fajfar P, Vidic T, Fischinger M. A measure of earthquake motion capacity to damage medium-period structures. Soil Dyn Earthq Eng 1990;9(5):236–42.

[42] Mackie K, Stojadinovic B. Seismic demands for performance-based design of bridges [PEER Report 2003/16]. Berkeley, CA: Pacific Earthquake Engineering Research Center, University of California; 2003.

[43] Von Thun J, Roehm L, Scott G, Wilson J. earthquake ground motions for design and analysis of dams. earthquake engineering and soil dynamics II—recent advances in ground-motion. Eval Geotech Spec Publ 1988;20:463–81.

[44] Housner GW. Spectrum intensities of strong motion earthquakes. In Proceedings of the symposium on strong motion earthquakes and blast effects on structures. Earthquake Engineering Research Institute, Los Angeles, CA; 1952.

[45] Housner GW. The behaviour of inverted pendulum structures during earthquakes. Bull Seismol Soc Am 1963;53(2):404–17.

[46] Bradley BA. Empirical equations for the prediction of displacement spectrum intensity and its correlation with other intensity measures. Soil Dyn Earthq Eng 2011;31(8):1182–91. http://dx.doi.org/10.1016/j.soildyn.2011.04.007.

[47] BSSC. NEHRP recommended provisions for seismic regulations for new buildings and other Structures [FEMA450, Part 2: commentary]. Washington, DC: Building

Seismic Safety Council; 2003.

[48] Trifunac MD, Brady AG. A study on the duration of strong earthquake ground motion. Bull Seismol Soc Am 1975;65(3):581–626.

[49] SAC Joint Venture. Proceedings of the invitational workshop on steel seismic issues. Report No. SAC 94-01, Los Angeles, CA; 1994.

[50] SAC Joint Venture. State of the art report on systems performance of steel moment resisting frames subject to earthquake ground shaking. Report No. FEMA 355C, Washington, DC; 2000 http://www.nehrp.gov/pdf/fema355c.pdf.

[51] Hall JF. Parameter study of the response of moment-resisting steel frame buildings to near-source ground motions [Report No. EERL 95-08]. Pasadena, CA: Earthquake Engineering Research Laboratory, California Institute of Technology; 1995.

[52] McKenna F, Fenves GL, Scott MH. OpenSees: open system for earthquake engineering simulation. Pacific earthquake engineering research center. Berkeley, CA: University of California; 2015.

[53] Kitayama S, Constantinou MC. Probabilistic collapse resistance and residual drift assessment of buildings with fluidic self-centering systems. Earthq Eng Struct Dyn 2016;45(12):1935–53. http://dx.doi.org/10.1002/eqe.2733.

[54] Newell JD, Uang CM. Cyclic behavior of steel wide-flange columns subjected to large drift. J Struct Eng 2008;134(8):1334–42. http://dx.doi.org/10.1061/(ASCE) 0733-9445(2008)134:8(1334).

[55] Lignos DG, Krawinkler H. Deterioration modeling of steel components in support of collapse prediction of steel moment frames under earthquake loading. J Struct Eng 2011;137(11):1291–302. http://dx.doi.org/10.1061/(ASCE)ST.1943-541X. 0000376.

[56] Yakhchalian M, Ghodrati Amiri G, Nicknam A. A new proxy for ground motion selection in seismic collapse assessment of tall buildings. Struct Des Tall Spec Build 2014;23(17):1275–93. http://dx.doi.org/10.1002/tal.1143.

[57] Tzimas AS, Kamaris GS, Karavasilis TL, Galasso C. Collapse risk and residual drift

performance of steel buildings using post-tensioned MRFs and viscous dampers in near-fault regions. Bull Earthq Eng 2016;14(6):1643–62. http://dx.doi.org/10. 1007/s10518-016-9898-3.

[58] Ang AHS, Tang WH. Probability concepts in engineering planning and design. Volume I—Basic Principles. NY: Wiley; 1975.

[59] Eads L. Seismic collapse risk assessment of buildings: effects of intensity measure selection and computational approach [Ph.D. dissertation]. Stanford, CA: Department of Civil and Environmental Engineering, Stanford University; 2013.

[60] Bradley BA. Site-specific and spatially distributed ground-motion prediction of acceleration spectrum intensity. Bull Seismol Soc Am 2010;100(2):792–801. http:// dx.doi.org/10.1785/0120090157.

[61] Bradley BA, Cubrinovski M, MacRae GA, Dhakal RP. Ground-motion prediction equation for SI based on spectral acceleration equations. Bull Seismol Soc Am 2009;99(1):277–85. http://dx.doi.org/10.1785/0120080044.

[62] Campbell KW, Bozorgnia Y. NGA ground motion model for the geometric mean horizontal component of PGA, PGV, PGD and 5% damped linear elastic response spectra for periods ranging from 0.01 to 10s. Earthq Spectra 2008;24(1):139–71. http://dx.doi.org/10.1193/1.2857546.

[63] Bommer JJ, Stafford PJ, Alarcón JE. Empirical equations for the prediction of the significant, bracketed and uniform duration of earthquake ground motion. Bull Seismol Soc Am 2009;99(6):3217–33. http://dx.doi.org/10.1785/0120080298.

[64] Baker JW, Jayaram N. Correlation of spectral acceleration values from NGA ground motion models. Earthq Spectra 2008;24(1):299–317. http://dx.doi.org/10.1193/1. 2857544.

[65] Bradley BA. Correlation of significant duration with amplitude and cumulative intensity measures and its use in ground motion selection. J Earthq Eng 2011;15(6):809–32. http://dx.doi.org/10.1080/13632469.2011.557140.